

## NEUROSCIENCE

# Dynamic regulation of vesicle pools in a detailed spatial model of the complete synaptic vesicle cycle

Andrew R. Gallimore<sup>1</sup>, Iain Hepburn<sup>1</sup>, Svilen V. Georgiev<sup>2</sup>, Silvio O. Rizzoli<sup>2\*</sup>, Erik De Schutter<sup>1\*</sup>

Synaptic transmission is driven by a complex cycle of vesicle docking, release, and recycling, maintained by distinct vesicle pools. However, the partitioning of vesicle pools and reserve pool recruitment remain poorly understood. We use a novel vesicle modeling technology to model the synaptic vesicle cycle in unprecedented molecular and spatial detail at a hippocampal synapse. Our model demonstrates robust recycling of synaptic vesicles that maintains consistent synaptic release, even during sustained high-frequency firing. We also show how the cytosolic proteins synapsin-1 and tomosyn-1 cooperate to regulate recruitment of reserve pool vesicles during sustained firing to maintain transmission, as well as the potential of selective vesicle active zone tethering to ensure rapid vesicle replenishment while minimizing reserve pool recruitment. We also monitored vesicle usage in isolated hippocampal neurons using pH-sensitive pHluorin, demonstrating that reserve vesicle recruitment depends on firing frequency, even at nonphysiologically high firing frequencies, as predicted by the model.

Copyright © 2025 The Authors, some rights reserved; exclusive licensee American Association for the Advancement of Science. No claim to original U.S. Government Works. Distributed under a Creative Commons Attribution NonCommercial License 4.0 (CC BY-NC).

## INTRODUCTION

Synaptic transmission is the fundamental mechanism of information transfer in the brain. Vesicles docked at the active zone rapidly fuse with the membrane in response to calcium influx following neural stimulation (1–3), driven by a complex signaling cascade involving membrane, vesicle, and cytosolic proteins (4, 5). These docked vesicles, primed for immediate release upon stimulation, form the readily releasable pool (RRP) (6, 7). However, the fidelity of sustained transmission with repeated stimulation relies on a reliable mechanism for the replenishment of the RRP as vesicles fuse with the membrane. The recycling pool—typically around 10 to 20% of the total vesicles—comprises freely diffusing vesicles available to refill empty docking sites following vesicle fusion (8–11). A (generally much larger) pool of vesicles—known as the reserve pool, comprises vesicles resistant to release, intermixed with vesicles of the recycling pool (11–14). Preassembled vesicle proteins on the presynaptic membrane form an additional readily retrievable pool (Fig. 1, A and B) (15, 16).

A typical hippocampal synaptic bouton contains 200 to 400 vesicles (17–19), which form a cluster maintained by intervesicle interactions between synapsin proteins on the vesicle surface (20–24). Following endocytosis, a vesicle becomes part of the recycling pool but slowly matures (over minutes to hours) and enters the reserve pool by becoming immobilized within the vesicle cluster by accumulation of synapsin (9, 25, 26). Synaptic activity causes synapsin dissociation from vesicles, controlled by protein kinase A (PKA; and CaMKII) phosphorylation (27) dispersing the cluster and mobilizing vesicles for release (Fig. 1, D to F) (28).

While the vesicle cluster plays an important role in maintaining vesicles within the bouton and restricting the availability of reserve vesicles for docking and release, the ability of vesicles to dock at the active zone is also modulated by the cytosolic protein tomosyn-1, which forms a complex with the small G protein, Rab3-GTP, blocking its critical docking interaction (29) with the active zone RIM1-Munc13

complex (30). Notably, synapsin interacts in a phosphorylation state-dependent manner with the Rab3-GTP-tomosyn-1 complex to form a tripartite complex. Cyclin-dependent kinase 5 (CDK5) phosphorylates tomosyn-1 and enhances its interaction with synapsin-1—this is counterbalanced by calcineurin (CaN)-dependent dephosphorylation (Fig. 1, E and F) (31, 32). This suggests a cooperative role of synapsin and tomosyn-1 in regulating the reserve pool using a combination of clustering and docking propensity to modulate the availability of vesicles for evoked release.

Although a regulated three-pool model is well accepted, many details are lacking. The characteristics of vesicles within the recycling and reserve pools, how they are partitioned, and the conditions under which vesicles are recruited from the reserve to the recycling pool remain poorly understood. Despite the increasing importance of computational modeling in understanding the behavior of complex emergent subcellular processes, such as long-term potentiation and depression (33–40), and synaptic vesicle release (41, 42), there are no published models of the synaptic vesicle cycle that incorporate the molecular mechanisms of vesicle transport, clustering, docking, priming, fusion, and recycling in a realistic spatial system. This is largely owing to a lack of technologies for modeling the complexities of vesicle structure and function. While voxel- and particle-based reaction-diffusion systems (43–45) are appropriate for modeling networks of simple molecules with negligible volume, they are completely unsuitable for modeling large, mobile, and heterogeneous structures such as synaptic vesicles, since their volume and molecular complexity have important roles in their function and influence their spatial dynamics and molecular interactions.

Our unique vesicle modeling technology extends the stochastic reaction-diffusion software, STochastic Engine for Pathway Simulation (STEPS) (43, 44), and allows us to model all key aspects of vesicle structure and function, including vesicle diffusion, the accumulation and diffusion of proteins on the vesicle surface, intervesicle protein-protein interactions (controlling vesicle clustering), vesicle-cytosolic protein-protein (and small molecule) interactions, vesicle-surface protein-protein interactions (controlling vesicle tethering and docking), and regulated endocytosis (vesicle recycling) and exocytosis (vesicle fusion and neurotransmitter release) (46). Each model vesicle

<sup>1</sup>Computational Neuroscience Unit, Okinawa Institute of Science and Technology Graduate University, Okinawa, Japan. <sup>2</sup>Department of Neuro- and Sensory Physiology, University Medical Center Göttingen, Germany.

\*Corresponding author. Email: srizzol@gwdg.de (S.O.R.); erik@oist.jp (E.D.S.)

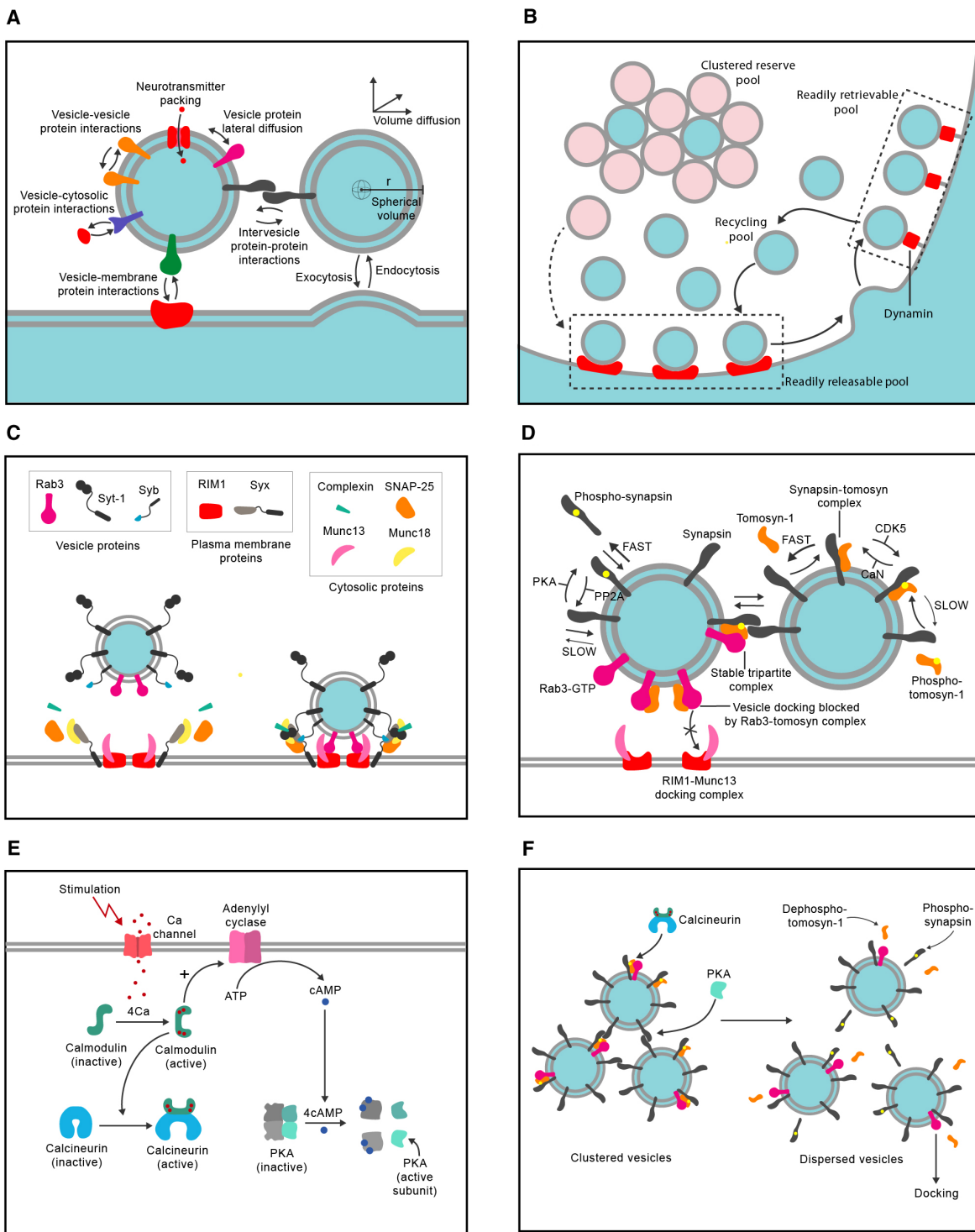


**Fig. 1. Structure of the vesicle and synaptic vesicle cycle model.** (A) All behaviors and interactions of our model vesicles. (B) Vesicle pools within the overall vesicle cycling model. (C) Docking and priming interactions represented in the vesicle cycling model (see Materials and Methods for details). Syt-1, synaptotagmin-1; Syb, synaptobrevin; Syx, syntaxin. (D) Interactions between synapsin-1, tomosyn-1, and Rab3 that govern vesicle clustering and docking propensity. CaN, calcineurin. (E) Stimulation-driven activation of CaN and PKA via Ca-mediated calmodulin activation. (F) Vesicles cluster by forming intervesicular bridges between synapsin molecules on the vesicle membrane. The dispersion of the vesicle cluster is driven by PKA-mediated phosphorylation of synapsin, which disrupts its interaction with the vesicle membrane and with other synapsin molecules. CaN-driven dephosphorylation of tomosyn-1 causes it to dissociate from the synapsin-Rab3-tomosyn tripartite complex, enabling the key Rab3-RIM interaction that drives vesicle docking at the active zone.

occupies an excluded diffusible spherical volume and unique position within the model tetrahedral mesh and, in addition to the external surface exposed to the cytosol, has an internal compartment for the packing and release of neurotransmitters and other small molecules (Fig. 1D). Using this technology, we were able to model all major phases of the synaptic vesicle cycle at unprecedented levels of molecular and spatial detail, from docking and priming to fusion and recycling, in a realistic synaptic bouton morphology reconstructed from electron micrographs (serial-sectioning transmission electron microscopy) of a cultured hippocampal pyramidal cell (Fig. 2A) (47). These phases of the vesicle cycle were modeled as stochastic reaction-diffusion models of both vesicle and plasma membrane proteins, as

well as diffusible cytosolic proteins and other small molecules. Docking, for example, is modeled by the interaction between the plasma membrane RIM1-Munc13 complex and vesicle membrane-bound Rab3-GTP. Formation of the SNAP receptor (SNARE) complex is then driven by interactions between the plasma membrane syntaxin-Munc18 complex and vesicle-bound synaptobrevin, with vesicle-bound synaptotagmin-1 and cytosolic complexin completing the fully primed SNARE complex (Fig. 1C and fig. S1). Vesicle release is then modeled as a regulated model exocytosis event triggered by binding of synaptotagmin-1 to cytosolic calcium ions, which enter the neuron via voltage-dependent Cav2.1 channel models tethered close to docking sites. Vesicle proteins deposited into the plasma

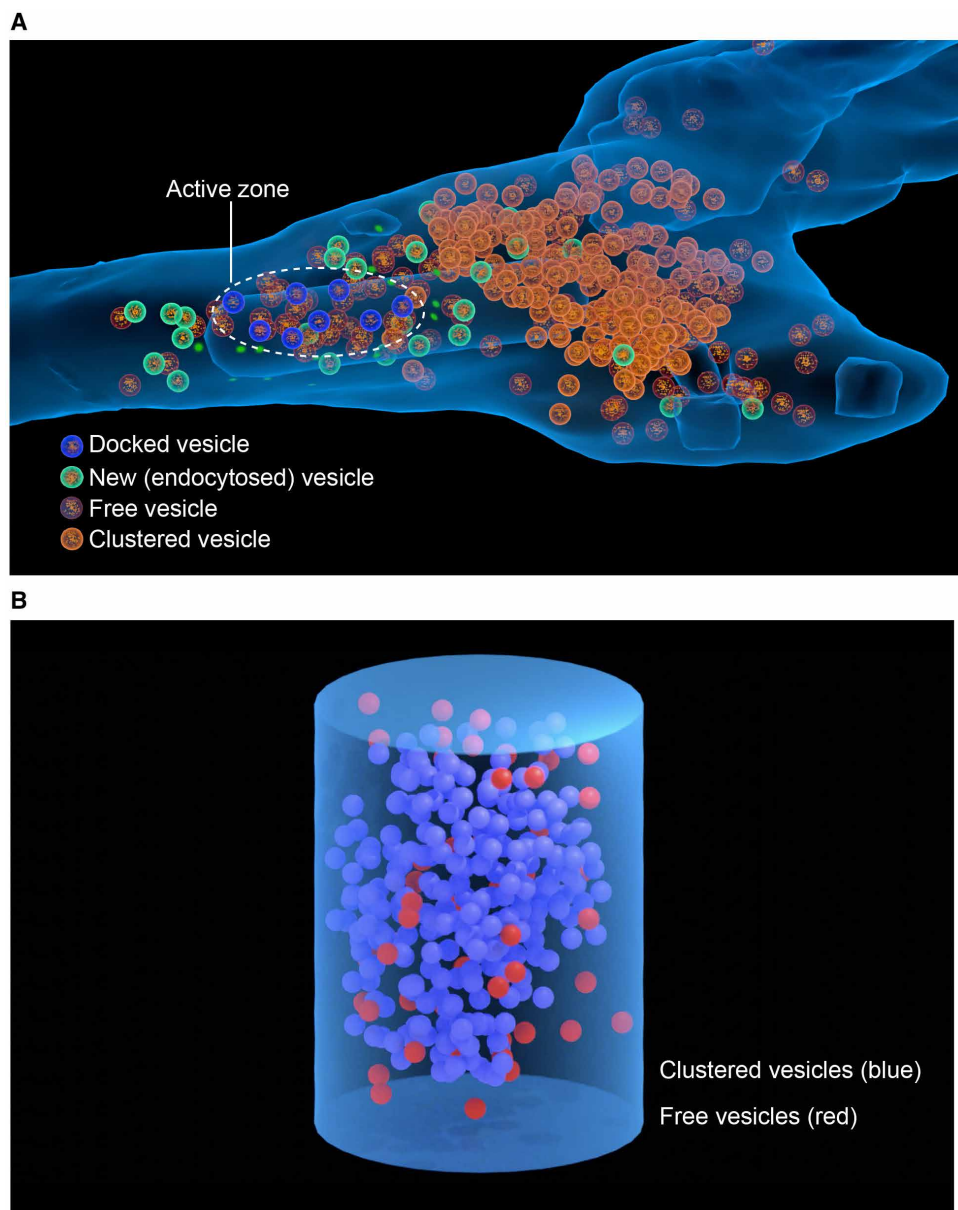


**Fig. 2. Blender visualization of the vesicle cycle model.** (A) Snapshot of complete vesicle cycling model showing clustered, free, newly endocytosed, and docked vesicles in the reconstructed synaptic bouton. (B) Toy model in a cylindrical mesh used to develop the vesicle clustering model. This toy model shows vesicle clustering behavior more clearly than the complete model in the hippocampal bouton reconstruction (see movie S1 for full animated visualization)

membrane during vesicle fusion are accumulated via adaptor proteins in preassembled vesicle pits, with vesicle retrieval modeled as an endocytosis event driven by dynamin. Intervesicle protein-protein interactions between vesicle-bound synapsin also successfully replicated the dynamic liquid phase behavior of the vesicle cluster (Fig. 2B and movie S1) (48, 49).

While hippocampal pyramidal cells fire at around 1 Hz during rest, this can increase to 5 to 20 Hz during periods of behavioral activity and be sustained for the duration of the activity (50, 51). Our model reveals highly dynamic and robust recycling of synaptic vesicles able to maintain stable and consistent synaptic release over time, even during such periods of high-frequency and sustained firing and assuming full vesicle collapse (as opposed to partial collapse proposed to occur during kiss and run recycling) followed by dispersal and retrieval of vesicle proteins. We also use our model to show how synapsin and tomosyn-1 can cooperate to regulate the recruitment of vesicles from the reserve pool during sustained periods of synaptic activity to maintain transmission, as well as the potential of selective vesicle tethering close to the active zone to ensure rapid vesicle replenishment and enhance the efficiency of the vesicle cycle by minimizing the recruitment of vesicles from the reserve pool. At all simulated stimulation frequencies studied, vesicle recycling was predominantly maintained by recycling vesicles, with recruitment from the reserve pool tightly regulated depending on stimulation frequency. On the basis of this model data suggesting that the degree of reserve vesicle recruitment is positively related to the frequency of neuronal firing (even at nonphysiologically high firing rates—above 20 Hz), we monitored vesicle usage in isolated hippocampal neuron cultures by labeling the vesicle lumen using pH-sensitive pHluorin, which fluoresces as vesicles fuse with the membrane and the lumen is neutralized. As predicted by the model, usage of reserve pool vesicles increased with stimulation frequency, even up to 50 Hz, helping to resolve a long-standing debate over the releasability of reserve pool vesicles in hippocampal neurons (8).

## RESULTS

### Endocytosis follows exocytosis closely, even at nonphysiological firing rates (model)

We first wanted to test whether our model vesicle cycling system could maintain synaptic transmission at increasing stimulation frequencies, up to and well beyond the maximum observed rate of around 20 Hz. Following an initial 5-s equilibration time, we simulated neural firing for 45 s at frequencies ranging from 5 to 50 Hz (averaged over 20 simulations at each stimulation frequency) (Fig. 3). As expected, the rate of vesicle fusion increased with stimulation frequency: At 5, 10, and 20 Hz, an initial rapid fusion rate (corresponding to release of the RRP) was followed by a slower and almost linear rate of vesicle release. However, at 50 Hz, a further acceleration of release was observed after ~15 s of simulated model stimulation (Fig. 3B). This effect could be blocked by selectively blocking tomosyn-1 dephosphorylation by CaN (fig. S3), demonstrating that this accelerated release is due to dephosphorylation of tomosyn-1, promoting dissociation of the synapsin–tomosyn-1 complex and thus liberation of vesicles from the reserve pool.

At all simulated stimulation frequencies studied, endocytosis followed exocytosis closely with a delay of ~2 to 3 s (Fig. 3A). The ratio of endocytosis:exocytosis remained between 0.84 and 0.87 at all frequencies from 5 to 50 Hz (52). This suggests that, even with the

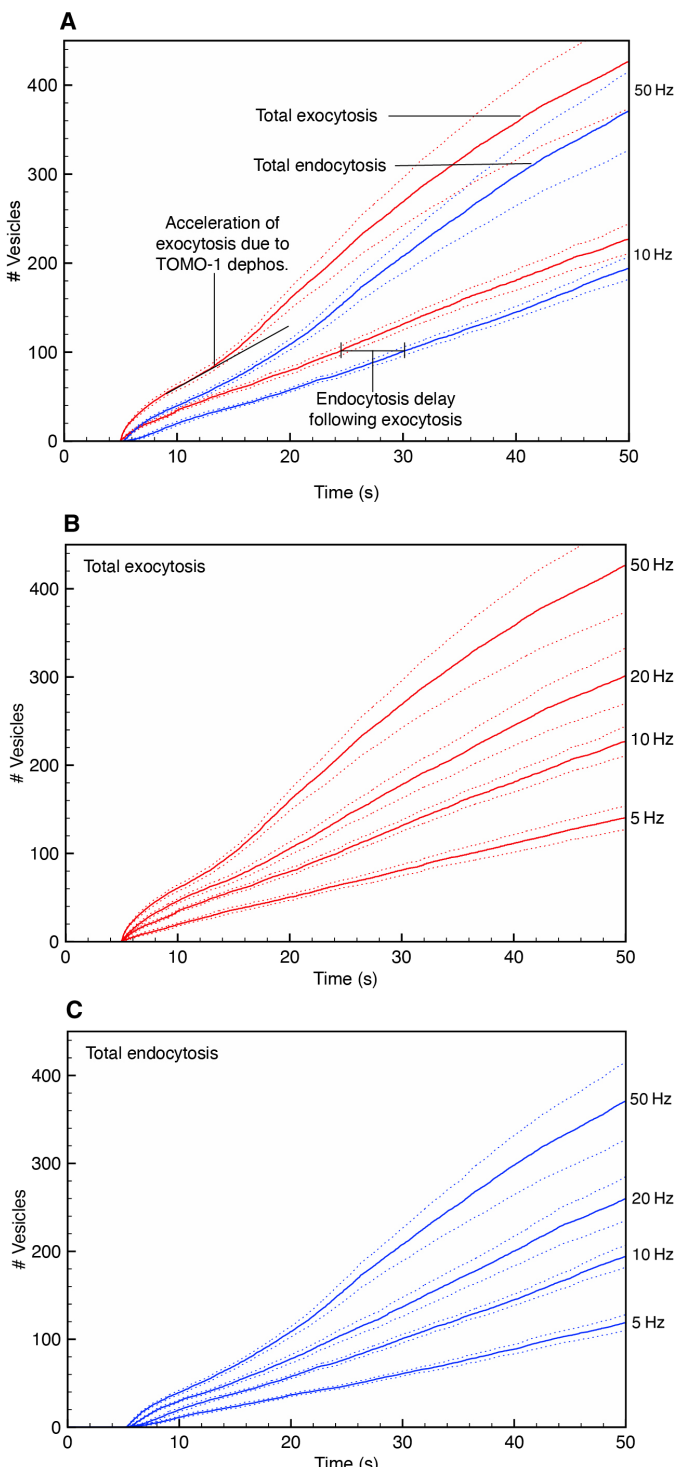


**Fig. 3. Synaptic vesicle release over time with frequency of stimulation.** (A) Total vesicle fusion and new vesicle endocytosis over time at 10 and 50 Hz (broken lines show 95% confidence interval). TOMO-1, tomosyn-1. (B) Total vesicle fusion over time at 5, 10, 20, and 50 Hz. (C) Total new vesicle endocytosis over time at 5, 10, 20, and 50 Hz.

assumption of dispersion and reaccumulation of vesicle proteins following exocytosis, the recycling system is capable of keeping pace with fusion at nonphysiologically high firing rates. This behavior

was not substantially affected by the position of the vesicle cluster, even when the vesicle cluster formed adjacent to the active zone (fig. S5), suggesting that the increased mobility and dispersion of the clustered vesicles during periods of extended high-frequency stimulation—when the greatest demands are being placed on the vesicle cycle—prevent clustered vesicles from interfering with vesicle recruitment, release, and retrieval.

### Vesicle material accumulates in the plasma membrane with increasing stimulation frequency (model)

Upon fusion at the active zone, the collapsed vesicle deposits its vesicular proteins, which include synaptotagmin-1 and synaptobrevin, into the plasma membrane, forming a “pit” of vesicle material. To further study the ability of the endocytic pathway to keep pace with vesicle fusion, we monitored the accumulation of this vesicle material in the membrane by recording the number of collapsed vesicles (pits) over the model simulation time. As the stimulation frequency increased, accumulation of vesicle material also increased, indicating that exocytosis was outpacing the rate at which vesicle material could be resequestered and vesicles recycled. This effect was particularly prominent at (nonphysiological) 50 Hz, with a 155% increase in vesicle material relative to baseline, compared to a 17% increase at 5 Hz (Fig. 4, A and C). This is comparable to experimental studies in hippocampal cells,

in which an accumulated membrane vesicle material was only observed to increase substantially with stimulation frequencies above 10 Hz (52).

Since dynamin-mediated scission is the final step in vesicle endocytosis (53–55) and considering that a maximum of 50 to 60 fully assembled dynamin complexes are available in a typical hippocampal bouton (18), we considered whether saturation of dynamin might account for this build-up of fused vesicle material in the plasma membrane. To test this in our model, we monitored the total number of dynamin complexes in use (bound to a fully assembled clathrin-coated pit) over time. In the initial state, we assumed that each clathrin-coated pit was bound to a dynamin complex and thus primed for endocytosis. Immediately following stimulation, the number of bound dynamin complexes dropped to ~40 to 60% of the initial number, indicating the endocytosis of vesicles from the readily retrievable pool (Fig. 4B). This number slowly increased as fused vesicles accumulated in the membrane and entered the readily retrievable pool. While the rate of accumulation of bound dynamin increased with the frequency of stimulation, it never reached the saturation threshold (i.e., when the maximum of 60 fully assembled dynamin complexes is reached), indicating that the number of dynamin complexes is not rate limiting in maintaining endocytosis within the timeframe of the simulation.

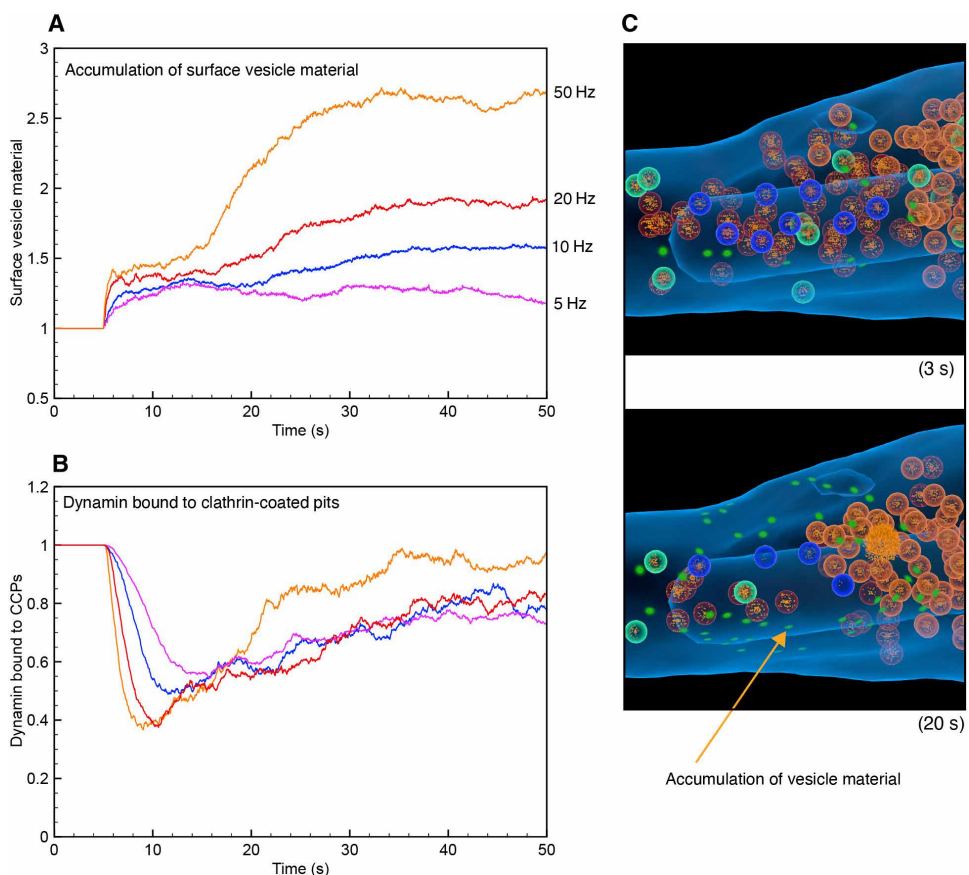


**Fig. 4. Accumulation of collapsed vesicle material (synaptotagmin-1 and synaptobrevin) in the plasma membrane.** (A) Accumulation of vesicle material in the membrane over time, at 5-, 10-, 20-, and 50-Hz stimulation. (B) Dynamin bound to clathrin-coated pits (normalized to the initial value) over time, at 5, 10, 20, and 50 Hz. (C) Accumulation of vesicle material is visible as green highlighted patches of membrane in the periactive zone area (stimulation at 50 Hz).

## Reserve vesicle usage as a function of stimulation frequency (model)

Since a build-up of vesicle material in the plasma membrane suggests a concomitant loss of recycling vesicles from the cytosol, the ability of the vesicle cycle to maintain an almost constant rate of vesicle release in our simulations, even at nonphysiologically high firing frequencies, suggested that vesicles must be being released from the reserve pool into the recycling pool. Without recruitment of reserve vesicles, recycling pool depletion would likely lead to a decrease in the rate of vesicle docking and fusion, threatening the continued fidelity of synaptic transmission. To test this, during the analysis, we partitioned fused vesicles into three types: vesicles from the initial recycling pool, vesicles from the initial reserve pool, and new vesicles formed by endocytosis. In experimental studies with cultured hippocampal neurons (56), ~75% of the initial recycling pool was used following 300 action potentials, compared to only 230 action potentials on our model. However, this can be accounted for by the relatively high release probability of our model. At 10 Hz, reserve vesicles remained unused until ~15 s of stimulation, and, at 45 s, ~20% of the reserve vesicles were used, compared to ~98% of the initial recycling pool. Most of the vesicles used at 45 s (~65%) were newly formed (i.e., endocytosed), indicating that vesicle recycling is largely responsible for maintaining vesicle release over time (Fig. 5C). Reserve vesicle usage increased with stimulation frequency, with only 9% of reserve vesicles being used at 5 Hz, increasing to 45% at 50 Hz (Fig. 5, A to C). This indicates that the regulated release of reserve vesicles (via both vesicle cluster dispersion and dephosphorylation of tomosyn-1, see below) is used to maintain the recycling pool as firing frequency increases.

## Reserve vesicle usage with stimulation frequency (isolated hippocampal neurons)

To test whether, as predicted by the model, recruitment and usage of reserve vesicle increased with firing frequency even up to high nonphysiological firing rates, we used pHluorin labeling to monitor release in isolated rat hippocampal neuron cultures. This technique uses a pH-sensitive nanobody-antibody complex to target the luminal domain of synaptotagmin-1, with the vesicle lumen being labeled while exposed to the culture medium during incubation with the nanobody-antibody complex. Upon fusion with the membrane, the vesicle lumen is neutralized, causing the pH-sensitive nanobody to fluoresce, which acts as a quantitative measure of vesicle exocytosis. However, since fused vesicles can be recycled by endocytosis, reacidified, and returned to the recycling pool, this technique alone does not distinguish between newly released vesicles (from the initial pools) and those that are released following a round of recycling. To overcome this limitation, we stimulated the neurons in the presence of bafilomycin, which prevents the reacidification of vesicles following endocytic retrieval from the membrane (57), and, as such, vesicles continue to fluoresce even after recycling and thus do not induce a change in fluorescence during any subsequent round of release. This allowed us to monitor changes in fluorescence specifically due to the release of vesicles initially present in the bouton and, as such, recruitment and usage of vesicles from the reserve pool.

To verify whether our procedures also label the reserve pool, we performed an experiment in which we labeled vesicles with the antibodies, as in all other experiments, and we then stimulated them in the presence of an anti-nanobody antibody (anti-VHH antibody,

where VHH stands for variable domain of a heavy chain-only antibody, meaning nanobody) that recognizes the pHluorin-conjugated nanobodies we used. Thereby, we label with the anti-VHH antibody all of the vesicles that participate in recycling during and after the stimulus (similar to experiments performed previously) (58). Vesicles that are not labeled during this procedure have become part of the reserve pool, since they do not respond to the respective stimulus. We relied on stimulating the synapses at 20 Hz, for 30 s, conditions that are designed to release the entire recycling pool in our cultures. As demonstrated in previous work (59), this stimulus is sufficient to exhaust all recycling vesicles, leading to the saturation of vesicle release (figure 3 of the respective work). As shown in fig. S6, a substantial pool of vesicles remains unlabeled, indicating that reserve vesicles are labeled in our conditions. At the same time, it is clear that a measurable proportion of the vesicle molecules is present on the surface membrane, under these conditions, as expected from previous works (26). This is not a problem for pHluorin imaging, since the baseline, provided by these vesicles and by the residual fluorescence of quenched pHluorin moieties within synapses, is subtracted in all measurements.

Stimulation of the cells for 30 s at 5 Hz in the presence of bafilomycin released 48% of the initially labeled vesicle pool, increasing to 63% at 10 Hz (Fig. 5, D and E, and fig. S7). Further increasing the stimulation frequency to 20 Hz did not cause a concomitant increase in vesicle usage, which remained at 63% of the initially labeled pools, indicating that stimulation at 10 Hz for 30 s is sufficient to release the entire recycling pool, with a reserve pool comprising 37% of the initially labeled pool remaining. We analyzed the bafilomycin values by a Friedman test ( $P < 0.00001$ ), followed by Tukey-Kramer post hoc tests. The 5-Hz stimulation result is significantly different from all others ( $P < 0.0001$ ). The 50-Hz stimulation result is also significantly different from all others ( $P < 0.01$  versus 10 or 20 Hz,  $P < 0.0001$  for 5 Hz). The 10- and 20-Hz results are not significantly different from each other ( $P = 0.9849$ ). This concurs with our model data, in which 98% of recycling vesicles were used with 45 s of stimulation at 10 Hz. However, by increasing the stimulation frequency to 50 Hz, vesicle usage increased to 74%, indicating that this supraphysiological high-frequency stimulation was able to recruit vesicles from this reserve pool, as predicted by our model (Fig. 5D). Compared to our model data, a substantially larger proportion of initial pool vesicles was used at all frequencies studied. However, the proportion of vesicles used is likely to depend on the total number of vesicles initially in the bouton, so it is likely that our model contains more vesicles than the mean number of bouton vesicles in the cultured cells studied.

## Dispersion of vesicle cluster is rapid and accompanied by a sharp increase in free tomosyn-1 (model)

The vesicle cluster exists as a liquid phase maintained by large numbers of intervesicle synapsin bridges (49). The binding of synapsin to vesicles and their cross-bridging are negatively regulated by PKA-mediated phosphorylation (27), and, as such, we predicted that sustained stimulation would disrupt the vesicle cluster and that this cluster dispersal would play an important role in releasing vesicles from the reserve pool into the recycling pool. To test this, we monitored the formation and dispersion of the vesicle cluster by counting the number of synapsin dimers between model vesicles. Vesicles lacking any dimers, and thus not connected to any other vesicles, were counted as free, whereas those with dimer connections were

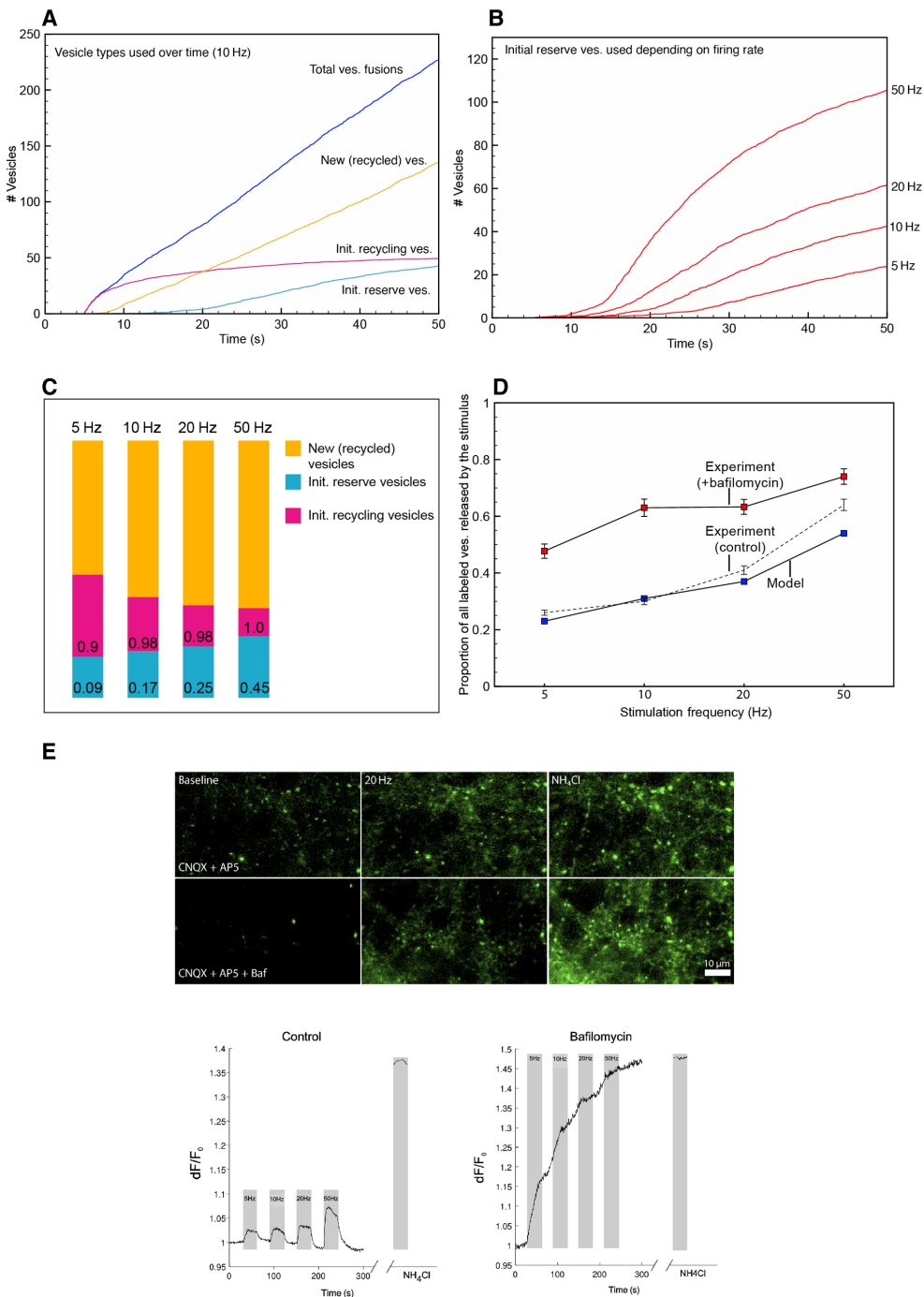


**Fig. 5. Usage of synaptic vesicles from different pools depending on stimulation frequency.** (A) Fusions of vesicle types during 10-Hz model stimulation (reserve and recycling vesicles are from the initial population, and new vesicles are those formed by endocytosis). (B) Usage of the model reserve vesicle pool at 5, 10, 20, and 50 Hz. (C) Proportion of vesicle types used after 45 s of model stimulation (5 to 50 Hz). Numbers indicate the fraction of the initial population of recycling (blue) and reserve (red) vesicles used. Note: Since there is no initial pool of recycled vesicles (yellow), no number is shown. (D) Comparison of initial vesicle pools (including all labeled vesicles within the cytosol) usage after 30 s of stimulation at 5, 10, 20, and 50 Hz in isolated hippocampal cells with vesicles prelabeled with pHluorin (experiment) and our model (i.e., sum of initial reserve and recycling vesicles used). The experiment control condition (broken line) does not include bafilomycin. (E) pHluorin imaging experiments. Neurons were incubated with an antibody against the luminal domain of synaptotagmin 1, decorated with secondary nanobodies conjugated to pHluorin. This tool is incorporated into recycling vesicles during the incubation time. The top shows the response of pHluorin-labeled vesicles to stimulation, comparing baseline condition (left) to a stimulation train of 20 Hz (30 s), and lastly to a pulse of NH<sub>4</sub>Cl, to neutralize the pH inside vesicles, and thereby reveal all pHluorin molecules. The bottom shows the same experiment but in the presence of bafilomycin, which inhibits vesicle reacidification. The bottom graphs indicate the fluorescence responses (normalized to the baseline) for the different conditions. Left: A series of stimulation trains was applied, at 5, 10, 20, and 50 Hz, before a final round of NH<sub>4</sub>Cl. Right: The same experiment, performed in the presence of bafilomycin. Average traces from individual experiments are shown. CNQX, cyanquinaline; AP5, (2R)-amino-5-phosphonopentanoate; Baf, bafilomycin.

considered part of the vesicle cluster (note that this definition of a free vesicle depends only on whether a vesicle is bound as part of the vesicle cluster. Whether a free vesicle becomes part of the recycling pool depends on its propensity for docking and release, which is also dependent on dissociation of the Rab3–tomosyn-1 complex). From the beginning of the simulation, the reserve vesicles became entirely clustered by ~5 s, driven by dimerization of synapsin and thus cross-linking of vesicles. The cluster remained completely intact with 7 s of 10-Hz stimulation (Fig. 6B and movie S2). The number of clustered reserve vesicles then declined to ~60% after 24 s of stimulation, before a rapid dissolution of the cluster over the following 3 s. At 50 Hz, cluster dispersion was complete by ~17 s of stimulation, driven by a faster rate of synapsin phosphorylation (Fig. 6, A and D). Since vesicle-bound synapsin forms a complex with tomosyn-1, cluster dispersion was accompanied by the release of tomosyn-1 from the vesicle surface, which depended on stimulation frequency, with up to ~67% of tomosyn-1 being released from vesicles at 50 Hz and ~30% at 10 Hz (Fig. 6B). This dispersion behavior is similar to that observed in frog motor terminals, in which vesicles remain immobile for ~15 s during 30-Hz stimulation, before a sharp increase in mobility, indicating rapid dispersal of the vesicle cluster (60). Blocking PKA-dependent phosphorylation of synapsin, and thus dispersal of the vesicle cluster, blocked reserve vesicle usage completely and reduced overall vesicle usage by 17% (at 10 Hz) (Fig. 6C).

### **Tomosyn-1 expression and vesicle clustering regulate the release of vesicles from the reserve pool (model)**

The cytosolic protein, tomosyn-1, forms a stable tripartite complex with synapsin and Rab3, which blocks the Rab3–RIM interaction required for vesicle docking at the active zone (31). We predicted that tomosyn-1 would play a role in regulating the propensity of vesicles released from the cluster to dock at the active zone, thus preventing cluster dispersion from rapidly releasing all reserve vesicles into the recycling pool and explaining the observed limited usage of reserve pool vesicles even after the vesicle cluster has dispersed. In hippocampal neuronal cultures, knockdown of tomosyn-1 causes a 30 to 50% increase in the apparent size of the total releasable pool of vesicles, whereas tomosyn-1 overexpression reduces this pool by ~25% (30). In our model, we observed similar responses to tomosyn-1 knockout and doubling the tomosyn-1 copy number. Relative to the control, the tomosyn-1-null model increased the total number of vesicles released from the initial recycling and reserve pools by 70% (Fig. 7A). However, this effect was entirely caused by an increase in reserve pool vesicle usage: The number of initial recycling pool vesicles used actually decreased by 18%. Usage of newly endocytosed (recycled) vesicles decreased by 33% in the tomosyn-1-null condition, indicating that the vesicle cycle was relying much more heavily on reserve pool vesicles to maintain synaptic release. However, the total number of vesicles used overall increased by 8%, owing to the absence of tomosyn-1's inhibitory effect on docking (Fig. 7B). Doubling the tomosyn-1 copy number had no substantial effect on the rate of vesicle release up to ~15 s of stimulation at 10 Hz. However, by strongly suppressing reserve pool vesicle usage and vesicle docking, the fusion rate then slowed, and the total vesicles used at 45 s was reduced by 29% (Fig. 7, A and B).

Together, these results indicate that tomosyn-1, by forming a stable tripartite complex with Rab3-GTP and synapsin, can restrict

the ability of reserve vesicles to dock at the active zone, even following cluster dispersion, and ensure that the vesicle cycle is maintained largely by newly endocytosed vesicles, thus avoiding unnecessary depletion of the reserve pool.

### **Selective tethering of vesicles near the surface membrane enhances the efficiency of the vesicle cycle (model)**

Long myosin V tethers are responsible for the initial recruitment and stabilization of vesicles near the presynaptic membrane (61) via a direct interaction between vesicle Rab3-GTP and the myosin tail (Fig. 8 and movie S3) (62–64). In our model, we model this myosin V tethering interaction by including “tethering paths” perpendicular to the membrane to which vesicles can bind and be directed to the membrane (see Materials and Methods). We surmised that the Rab3–myosin V interaction, like the Rab3–RIM interaction, is likely to be inhibited by the binding of tomosyn-1, thus providing a mechanism for the selective tethering of vesicles with free Rab3-GTP (unbound to tomosyn-1) close to the presynaptic membrane. Hence, we include a requirement for vesicles to contain free Rab3 on the vesicle membrane surface to bind the tethering path. This selective tethering was used in all model simulations.

In experimental studies, disruption of the myosin V tethers resulted in a 50% reduction in vesicle usage (65). In our model, removing the tethering paths entirely reduced the rate of vesicle fusion throughout the stimulation period and the total number of fusion events after 45 s of 10-Hz stimulation by 28% (Fig. 7A). We hypothesized that this selective tethering ought to improve the efficiency of the vesicle cycle by selectively recruiting recycling vesicles and vesicles released from the cluster with docking propensity, as well as preventing the occlusion of docking sites by vesicles unable to form the crucial Rab3–RIM docking interaction. To test this, we removed the Rab3 dependency in the tethering interaction in our model, such that all vesicles could attach to a tethering path whether they contain free (unbound to tomosyn-1) Rab3. Compared to Rab3-dependent selective tethering, nonselective tethering reduced the overall number of vesicles released after 45 s of 10-Hz stimulation by 13% while simultaneously increasing the number of reserve vesicles used by 48% (Fig. 7A).

### **DISCUSSION**

Our detailed spatial model of the complete vesicle cycle reveals how a complex interplay of vesicle and cytosolic proteins, molecular tethering at the plasma membrane, and the maintenance of a dynamic vesicle cluster generate a remarkably robust recycling system, able to maintain vesicle release at frequencies well beyond what could be considered physiological for hippocampal neurons. In particular, we show how Rab3, synapsin-1, and tomosyn-1 can potentially work together to maintain and regulate the release of vesicles from the vesicle cluster and their propensity for release, thus providing a mechanism for the dynamic segregation of the recycling and reserve pools depending on need (30). Furthermore, we show how selective tethering of vesicles at the active zone can improve the efficiency of the vesicle cycle by preventing the docking of vesicles with a low propensity for release and reducing the number of vesicles recruited from the reserve pool. Also, despite its limited availability, saturation of dynamin—controlling the final step in endocytosis—appears unlikely to be an issue even at nonphysiological firing frequencies for up to a minute.

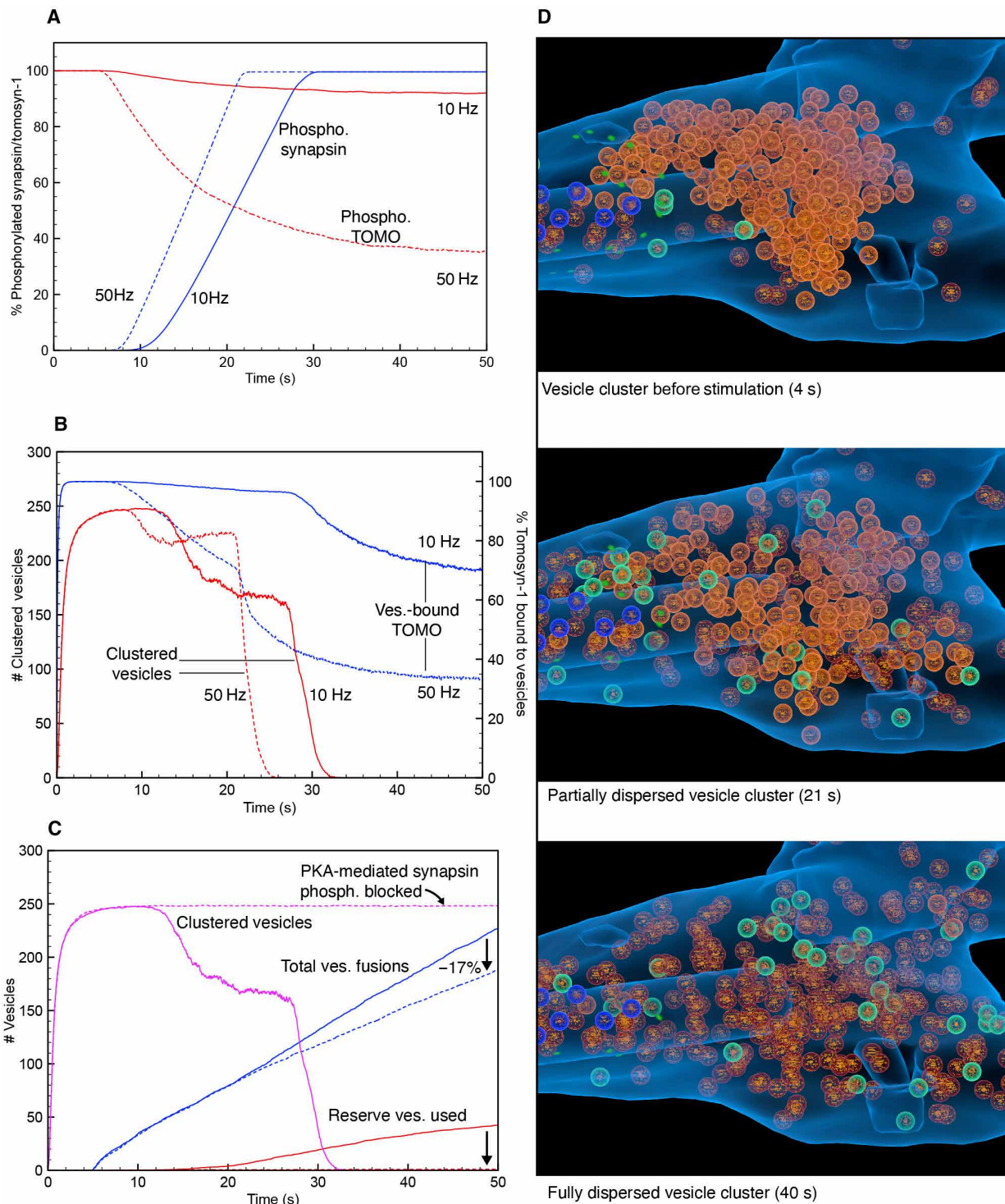


**Fig. 6. Regulation of vesicle clustering and dispersion by synapsin-1 and tomosyn-1.** (A) Phosphorylation of synapsin1 and tomosyn-1 (TOMO) over time at 10- and 50-Hz model stimulation over 45 s. (B) Vesicle cluster formation and dispersal and tomosyn-1 bound to vesicles over time at 10- and 50-Hz model stimulation beginning at 5 s. (C) Effect of blocking cluster dispersion (by blocking PKA-mediated synapsin phosphorylation—dashed line) on vesicle fusion and reserve vesicle usage with 10-Hz model stimulation. (D) Progression of vesicle cluster dispersal over time with 50-Hz model stimulation (see movie S2).

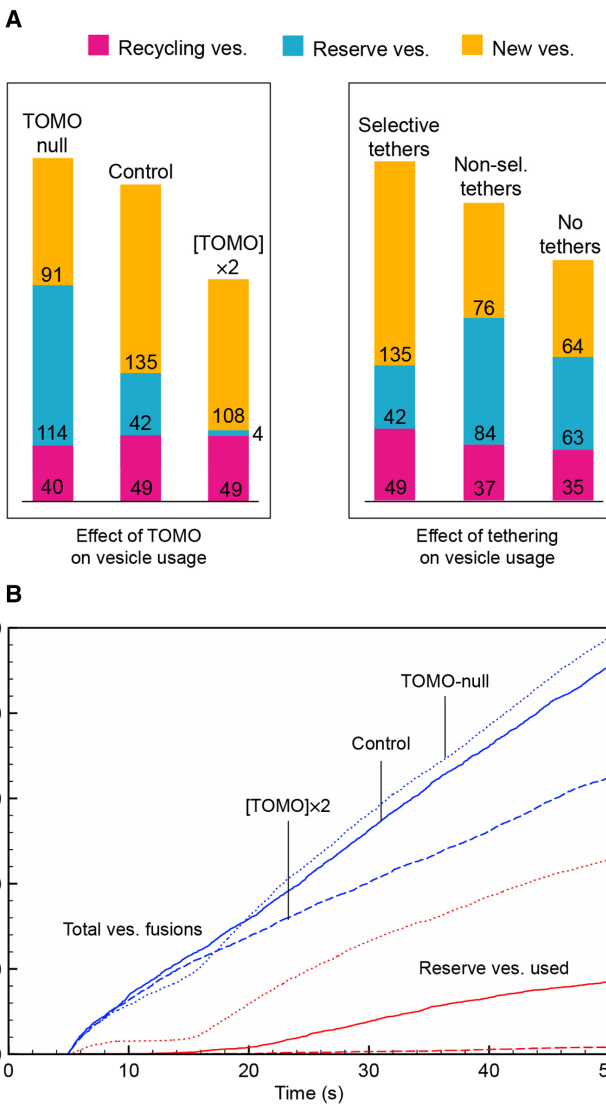


**Fig. 7. Effect of tomosyn-1 and tethering on synaptic vesicle usage.** (A) Effect of tomosyn-1 (TOMO) copy number, selective and nonselective tethering on vesicle usage after 45 s of model stimulation at 10 Hz. Left: Effect of tomosyn-1 copy number of the absolute number of vesicles used from each pool. Numbers represent number of vesicles used after 45 s of stimulation). Right: Effect of tethering (selective and nonselective) on the absolute number of vesicle types used from each pool. (B) Effect of tomosyn-1 copy number on the total vesicle fusion and reserve vesicle usage over time at 10 Hz.

At all simulated stimulation frequencies studied, endocytosis followed exocytosis closely, and, following depletion of the recycling pool, most of the fusion events were from recycled vesicles, indicating that vesicle recycling is mainly responsible for maintaining synaptic transmission over time. This dovetails with experimental studies demonstrating that, at relatively low frequencies, recycling can be maintained using only a small proportion of the entire vesicle pool (11, 13, 66), as well as a study showing that newly endocytosed vesicles are preferentially used over more mature vesicles (26). However, as the firing rate and stimulation time increase, the recycling pathway becomes overwhelmed and is unable to compensate for the rapid rate of vesicle fusion: The recycling pool is depleted, and the

vesicle material begins to accumulate in the membrane. In the absence of a reserve pool, this would lead to a gradual decrease in release probability, threatening the fidelity of synaptic transmission. However, dispersion of the vesicle cluster, together with CaN-mediated dephosphorylation of tomosyn-1 and destabilization of the Rab3-tomasyn-synapsin tripartite complex, releases vesicles from the reserve pool for docking and fusion. Once a reserve vesicle is used and recycled, it becomes a part of—and thus increases the size of—the recycling pool, further increasing the availability of vesicles for release without the requirement for direct coupling of exocytosis and endocytosis. The purpose of the reserve pool is not simply to supply additional vesicles when the recycling pool is depleted but to release vesicles into the vesicle cycle and increase the number of actively recycling vesicles (following fusion and retrieval), which allows the cycle to maintain a higher rate of fusion and retrieval over time.

Previous studies in isolated hippocampal neuron cultures have indicated that vesicles from the reserve pool are highly resistant to release, even during periods of intense stimulation, and it remains a matter of debate whether they are ever recruited *in vivo* (6). However, our model predicted that reserve vesicle recruitment and usage should increase with the frequency of stimulation, even well beyond physiological firing rates. We were able to demonstrate this in isolated hippocampal neuron cultures by monitoring vesicle release using pH-sensitive pHluorin labeling, which revealed recruitment and usage of vesicles from the reserve pool at stimulation frequencies up to 50 Hz, in line with our model predictions.

Although considering vesicles as being part of separate recycling and reserve pools is an instructive simplification, the distinction between the recycling and reserve vesicle pools does not appear to be sharply delineated (9). In hippocampal neurons, all vesicles, including those of the putative reserve pool, will eventually fuse during mild stimulation over extended periods of time (9, 17). This suggests that the likelihood of a particular vesicle being used is largely probabilistic, with the recycling pool simply comprising those vesicles with a relatively high propensity for docking and release, although this propensity can change as a vesicle matures or, as we have shown, dependent on synaptic activity and the pattern of vesicle protein phosphorylation (26). The transition from the recycling to the reserve status may be faster (hours) than assumed by a previous study that only tested time points at or above 12 hours (26).

While it is ostensibly reasonable to suppose that release of vesicles from the cluster is alone responsible for rendering them available for docking and release, effectively transferring them from the reserve to the recycling pool, the vesicle cluster often lies close to the active zone, and both types of vesicles are intermixed. Hence, clustering alone is unlikely to provide control over pool segregation and recruitment. However, synapsin-1 and tomosyn-1 can work together to both maintain the population of reserve vesicles within the synaptic bouton and to control their propensity for fusion and thus, following retrieval, release into the recycling pool. By forming a stable tripartite complex, Rab3, tomosyn-1, and synapsin-1 can lock vesicles in a nonfusion-competent state within the vesicle cluster. PKA-mediated phosphorylation of synapsin causes dispersal of the vesicle cluster and promotes loss of tomosyn-1 from Rab3, effectively releasing vesicles from the reserve pool. At high firing rates, this is further promoted by CaN-dependent dephosphorylation of tomosyn-1, which disrupts the tomosyn-1–synapsin interaction. Although our model shows that tomosyn-1 does not appear

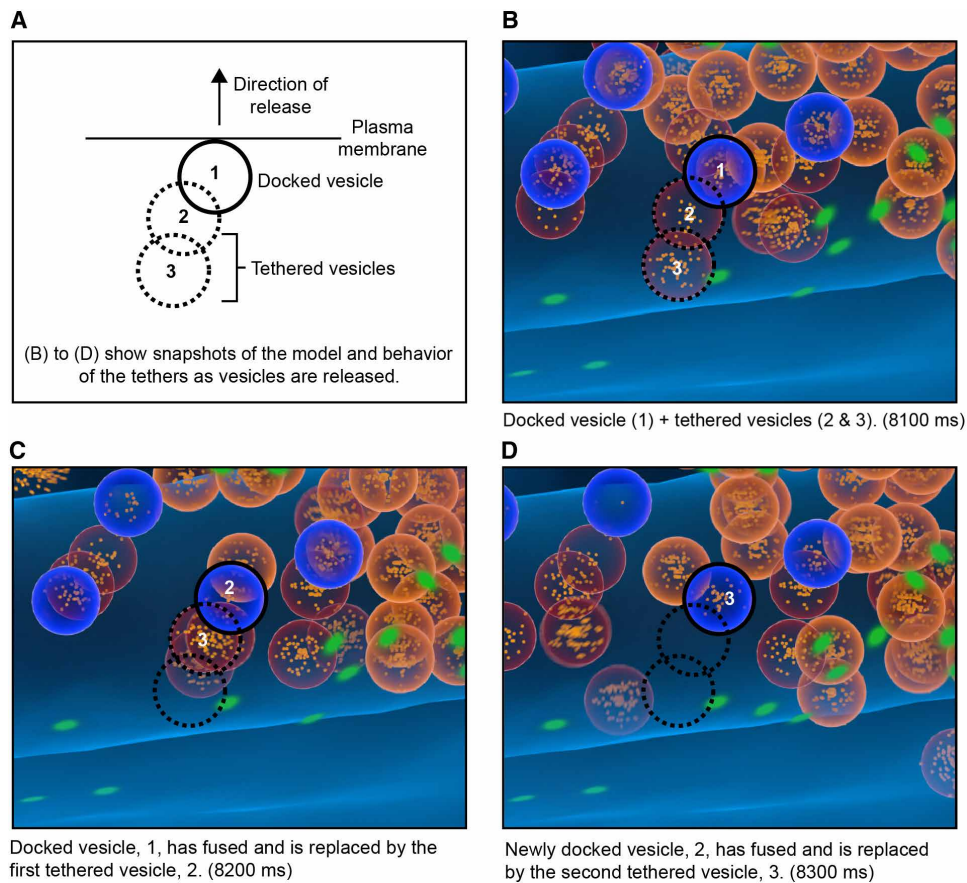


**Fig. 8. Blender visualization of vesicle tethering.** (A) Schematic showing tethered vesicles behind a single docked vesicle. (B) Snapshot of model showing the tethered vesicles behind a single docked vesicle (see movie S3). (C) As a docked vesicle fuses, it is replaced by a tethered vesicle which moves into the vacant docking site. (D) The newly docked vesicle fuses and is replaced the next tethered vesicle (the fusion and replacement of docked vesicles is more clearly seen in movie S3).

to regulate the overall availability of vesicles for release, it is able to control the proportion of vesicles from the reserve pool that are used. Blocking PKA-mediated dispersion of the cluster or increasing tomosyn-1 copy number prevents reserve vesicle recruitment and compromises vesicle release at higher firing rates.

In addition to efficient recycling of vesicle material following exocytosis, stable vesicle release also depends on the rapid replenishment of vacant docking sites. While recycling vesicles are observed to diffuse freely through the cytosol, intermixing with the vesicle cluster, relying on random diffusion alone to bring vesicles close to the active zone docking sites is likely to be inefficient in replenishing fused vesicles. In addition, long myosin V tethers are responsible for initial recruitment and stabilization of vesicles much further from the membrane (61), ensuring that the RRP can be replenished in a timely manner during repetitive stimulation, with myosin V disruption resulting in a 50% reduction in vesicle usage in experimental studies (65) and by 28% in our model. Since both the recycling and reserve pool vesicles are packed into the bouton close to the active zone (14, 22), it is likely that tethering should be somewhat selective for recycling pool vesicles to avoid clogging the active zone with reserve vesicles that are not viable for release. In addition, since Rab3-GTP interacts with myosin V (potentially via an unidentified effector protein) (63, 67), it is plausible that this long-distance tethering is also dependent on free Rab3-GTP. Once a

vesicle is moved to the docking site, Rab3–myosin V interactions can be displaced by the Rab3-RIM1-Munc13 docking interactions. In support of this model, selective tethering both enhances the rate of vesicle release over time while also reducing the number of vesicles recruited from the reserve pool to maintain synaptic release. Reserve pool vesicle recruitment is not cost free, since released vesicles must ultimately be returned to the reserve pool cluster by the slow accumulation of synapsin to avoid being lost from the bouton. Selective tethering allows a smaller number of recycling vesicles to maintain the vesicle cycle with minimal reserve pool recruitment at physiological firing rates.

While our model captures all phases of the vesicle cycle, it is by no means complete. For example, we do not take into account possible involvement of “superprimed” vesicles (68), nor tomosyn-1’s role in inhibiting vesicle priming by antagonizing Munc13 and inhibiting SNARE complex formation (69–73). Also, we only model the most prominent form of recycling involving full vesicle collapse and retrieval, but we do not consider very fast (<1 s) recycling events, which likely represent vesicle retrieval without full vesicle collapse (“kiss and run”) (74), nor bulk endocytosis. It is estimated that the kiss and run mode is used in around 20% of hippocampal vesicle release events (75). However, since kiss and run only requires the transient exposure of the vesicle interior and obviates the requirement for vesicle protein dispersal and reaccumulation, this

mode is certainly more efficient than the clathrin-mediated recycling involving full vesicle collapse and retrieval. Likewise, bulk endocytosis is generally triggered during periods of intense stimulation that threaten to overwhelm the vesicle cycle and, as such, works to increase the efficiency of the vesicle cycle (76, 77). Hence, the real hippocampal vesicle recycling system is likely to be even more efficient than indicated by our model. Since we only model a hippocampal en passant synapse, it is not clear how generalizable our results are to other types of neurons and synapses. However, our unique vesicle modeling technology will provide rich opportunities for studying other neuron and synapse types, as well as other mechanisms involved in the highly complex and dynamic regulation of the synaptic vesicle cycle.

## MATERIALS AND METHODS

### Structure of the vesicle recycling model

The synaptic bouton morphology was constructed as a tetrahedral mesh using Meshlab and our MultiCompMesher (78) derived from an electron micrograph reconstruction of a cultured hippocampal neuron en passant synapse, which also provided the location and the area of the active zone (47). Cytosolic and vesicle protein copy numbers were derived (where available) from Wilhelm *et al.* (18), with cytosolic and membrane diffusion rates taken from Reshetniak *et al.* (47).

Broadly, the synaptic bouton was initially populated with 300 model vesicles (initial recycling pool: 50; reserve pool: 250—further details below) freely diffusible within the cytosol. The cytosol was also populated by the freely diffusible cytosolic proteins: complexin-1, Munc18, Munc13, Rab3, α-SNAP, N-ethylmaleimide-sensitive factor (NSF), dynamin, calmodulin, CaN, CDK5, syndapin, tomosyn-1, and synapsin. The plasma membrane was populated by the membrane proteins syntaxin and SNAP-25, which are free to diffuse within the membrane surface. As well as diffusing through the cytosol, vesicles can dock at the active zone (via the RIM-Munc13 complex—see below), fuse with the membrane and be recycled via endocytosis, completing the vesicle cycle. Clustering of vesicles occurs via interactions between vesicle-bound synapsin.

### Simulation of synaptic stimulation

All simulations were run on a prerelease version of STEPS 5, which passed all validations presented in (46). The hardware used was the “Deigo” cluster at the Okinawa Institute of Science and Technology, on nodes consisting of  $2 \times 64$  Advanced Micro Devices, Inc. (AMD) Epyc 7702 at 2.0-GHz cores. The model performance was found to peak at around 256 cores (46), so each individual simulation was run on two full AMD nodes. For 50-s model time, each simulation took approximately 10 days. Model code is available on the ModelDB site (<https://modeldb.science/2018007>).

All simulations were run for 5 s of model time to reach steady state (to allow vesicle docking, clustering, etc.), followed by 45 s of stimulation at varying frequencies (5, 10, 20, and 50 Hz). Action potentials were simulated by instantaneous reversal of the membrane potential from  $-60$  to  $40$  mV for 1 ms. Model species, reactions, parameters, and diffusion rates are detailed in tables S1 to S4.

### Modeling of the initial vesicle populations

All vesicles were populated with vesicle proteins synaptobrevin, synaptotagmin-1, and Rab3-GTP. In addition, to model the buffering of other recycling proteins, vesicles also contain binding sites for

complexin, Munc13/18, syndapin, α-SNAP, and NSF (79), with on/off rates tuned to fit the measured proportions of proteins bound to the vesicle cluster (47). All vesicle proteins could diffuse freely within the vesicle membrane. The only distinction between reserve (initial population: 250) and recycling pool (initial population: 50) vesicles is that the former each contained 10 binding sites for synapsin-1 (Fig. 1A) (80). Such that they did not accumulate synapsin-1 in the timeframe of the simulation (25), recycling vesicles (and newly formed vesicles which become part of the recycling pool (81)) contained no synapsin-1 binding sites. A single vesicle was placed at each docking site at the beginning of the simulation to allow rapid docking and population of the RRP. The readily retrievable pool was populated with 40 clathrin-coated pits containing the full complement of vesicle proteins including dynamin (82).

### Modeling of vesicle docking

The active zone, with an area of  $0.060 \mu\text{m}^2$  [within the range measured by ultrastructural analysis of hippocampal synapses (83)] was populated with eight vesicle docking sites constructed from static RIM1-Munc13 clusters (84–87) within the active zone (88–90). Calcium channel tethering was modeled by placing four Cav2.1 channels (91) in neighboring membrane triangles (92).

Vesicle docking is driven by the interaction between vesicle surface Rab3-GTP and the RIM-Munc13 complex. RIM-1 forms a complex with Munc13 which is essential for docking (Fig. 1B and fig. S1). RIM-1, Munc13, and Rab3-GTP form a tripartite complex which drives docking (84–87). Tomosyn-1 binds Rab3-GTP on vesicles, forming a complex that is unable to bind to the RIM1-Munc13 complex, thus preventing docking (Fig. 1C). Tomosyn-1 is phosphorylated by CDK5 and dephosphorylated by CaN, with the dephosphorylated form dissociating more rapidly from Rab3-GTP (30).

### Modeling of selective vesicle tethering

Tether paths of length 100 nm (allowing one to two vesicles to be tethered behind the docked vesicle) were placed at the center along the normal of each docking site (65, 93). Only vesicles containing free Rab3-GTP (not complexed with tomosyn-1) on the vesicle for tethering (to model the Rab3-GTP-myosin V interaction) can bind to the tether (this “selective tethering” is the control condition used in all simulations, except where otherwise stated) (67). Once attached to a tether path, vesicles will move along the path until reaching the membrane (unless blocked by another docked or tethered vesicle), mimicking retraction of the tether to draw the vesicle into the docking site.

### Modeling of vesicle priming

Munc18 binds tightly to syntaxin-1, locking it into a closed conformation and preventing extraneous binding to SNAP-25 (Fig. 1B and fig. S1) (94, 95). Munc13 catalyzes the transfer of the Syntaxin-Munc18 complex into the SNARE complex (binding to SNAP-25) (94–96). For kinetics, see Zikich *et al.* (97). Synaptobrevin (vesicle) is then incorporated into the complex to form the complete SNARE complex (98, 99). Vesicle synaptotagmin-1 binds to the SNARE complex, followed by complexin (2), fully priming the vesicle for  $\text{Ca}^{2+}$ -triggered fusion.

### Modeling of vesicle fusion (exocytosis)

Synaptotagmin-1 comprises two domains (C2A binds three  $\text{Ca}^{2+}$ , and C2B binds two  $\text{Ca}^{2+}$ ) (100, 101). All five  $\text{Ca}$  sites must be occupied to

trigger the conformational change that drives vesicle fusion. The binding of  $\text{Ca}^{2+}$  to synaptotagmin-1 was calibrated against experimental data described in (100) (fig. S4). Upon  $\text{Ca}$ -triggered fusion (an exocytosis event in STEPS), any neurotransmitter in the vesicle lumen is expelled into the extracellular space, and all vesicle membrane proteins (synaptotagmin, synaptobrevin, and Rab3) are deposited into the presynaptic plasma membrane and can freely diffuse in the plasma membrane for use in reassembly of vesicle pits for vesicle recycling (see “postfusion” below).

### Measurement of release probability and recycling time in the recycling model

At hippocampal synapses, release probability (the probability of at least one vesicle fusion event following a single action potential) can vary greatly, with most synapses in the range of 0.1 to 0.6 (102–104) and largely dependent on the number of calcium channels coupled to each docking site (104–106). Our model displayed a release probability of 0.5 and, as such, sits toward the higher end of this range. However, modeling a relatively high release probability synapse provided a better opportunity to model vesicle cycle dynamics within model simulation times that were feasible to compute.

The time taken for fused vesicles to be retrieved from the membrane (recycling time) varies depending on neuron type and is regulated at a cell-wide level (107), following an exponential distribution with a mean time, in hippocampal neurons, ranging from ~5 to 40 s (53, 107). In our model, we measured the recycling time following 500 simulated fusion events and observed recycling times between 2.5 and 18.6 s, with a mean time of 6.8 s and within the range observed experimentally (fig. S2). While our model does not account for the time required for neurotransmitter refilling following vesicle endocytosis, proton gradient–driven neurotransmitter packing proceeds with similar kinetics to endocytosis [ $\tau \approx 15$  s for glutamate via Vesicle Glutamate Transporter (VGLUT)] (108, 109), and, following vesicle retrieval, newly retrieved vesicles have been shown to exhibit the same propensity for release as existing vesicles (56), suggesting that neurotransmitter packing is unlikely to be rate limiting.

### Modeling the postfusion vesicle processing

Following fusion with the membrane, the vesicular proteins synaptotagmin and synaptobrevin disperse (within the bouton plasma membrane only) (110, 111). Each vesicle fusion event triggers the generation of a new pit in a random position in the endocytic zone surrounding the active zone for the reaccumulation of dispersed vesicle proteins (112). The cis-SNARE complex is dismantled by NSF/ $\alpha$ -SNAP (113, 114). This is a slow, possibly multistep reaction taking ~6 s per SNARE complex (115).

### Modeling of vesicle retrieval and recycling

Newly formed pits contain adaptors for synaptotagmin-1 (AP2) and synaptobrevin (AP180), which bind and accumulate these vesicle proteins in the readily retrievable pool following vesicle fusion and protein dispersion (111) [protein reclustering times fitted to data from (111)]. As well as triggering vesicle fusion,  $\text{Ca}^{2+}$  also activates CaN (via calmodulin). Active CaN dephosphorylates (and thus activates) dynamin. Active dynamin is responsible for the last step in endocytosis of vesicles from the readily retrievable pool (15, 53). Only pits with their full complement of synaptotagmin-1, synaptobrevin, and Rab3-GTP can be retrieved from the readily retrievable

pool. Once formed, the newly retrieved vesicles become part of the recycling pool and can dock and fuse at the active zone.

### Modeling of vesicle clustering

Reversible binding interactions between cytosolic synapsin and the model vesicle membrane causes synapsin to accumulate on the vesicle surface (116, 117), and synapsin-synapsin interactions cause vesicles to cluster (27). Vesicle clustering is not dependent on synapsin-actin interactions (60), but static actin proteins in the cytosol act as seeds for the vesicle cluster. Synapsin-1 is phosphorylated by PKA and dephosphorylated by PP2A (Fig. 1C). The phosphorylated form of synapsin-1 dissociates more rapidly from both the vesicles and into the monomeric form (110, 118, 119). Vesicle-bound synapsin-1 also forms a stable heterotrimer with the tomosyn-Rab3-GTP complex (30).

### Animal usage in experimental work

All used animals were handled according to the regulations of the local authorities, the State of Lower Saxony (Landesamt für Verbraucherschutz, Braunschweig, Germany) and of the University of Göttingen. All animal experiments were carried out in accordance with the European Communities Council Directive (2010/63/EU) and approved by the local authority, the Lower Saxony State Office for Consumer Protection and Food Safety (Niedersächsisches Landesamt für Verbraucherschutz und Lebensmittelsicherheit).

### Preparation of rat dissociated hippocampal cultures

For the preparation of dissociated primary hippocampal cultures, newborn rats (*Rattus norvegicus*) were used, following previously established methods (120, 121). Briefly, hippocampi of newborn rat pups (wild-type, Wistar) were dissected in Hanks' balanced salt solution (5 mM KCl, 140 mM NaCl, 4 mM  $\text{NaHCO}_3$ , 6 mM glucose, 0.4 mM  $\text{KH}_2\text{PO}_4$ , and 0.3 mM  $\text{Na}_2\text{HPO}_4$ ) and incubated for 60 min in enzyme solution [Dulbecco's modified Eagle's medium (DMEM; #D5671, Sigma-Aldrich, Germany), containing 100 mM  $\text{CaCl}_2$ , 50 mM EDTA, cysteine (0.5 mg/ml), and papain (2.5 U/ml), saturated with carbogen for 10 min]. The dissected hippocampi were subsequently incubated for 15 min in a deactivating solution [DMEM containing bovine serum albumin (0.2 mg/ml), 5% fetal calf serum, and trypsin inhibitor (0.2 mg/ml)]. The cells were then triturated and seeded on circular glass coverslips with a diameter of 18 mm at a density of approximately 80,000 cells per coverslip. Before seeding, all coverslips underwent treatment with nitric acid, sterilization, and coating overnight with poly-L-lysine (1 mg/ml). The neurons were allowed to adhere to the coverslips for 1 to 4 hours at 37°C in plating medium (DMEM containing 2 mM glutamine, 3.3 mM glucose, and 10% horse serum). Subsequently, the medium was switched to neurobasal-A medium (Life Technologies, Carlsbad, CA, USA) containing 1% GlutaMAX (Gibco, Thermo Fisher Scientific, USA), 2% B27 (Gibco, Thermo Fisher Scientific, USA) supplement, and 0.2% penicillin/streptomycin mixture (Biozym Scientific, Germany). The cultures were then incubated at 37°C and 5%  $\text{CO}_2$  for 13 to 15 days before use. If the pH indicator suggested a loss of medium quality, then the culture medium was renewed (at most once per week, to avoid disturbing the cultures). Percentages represent volume/volume.

### Hippocampal vesicle labeling

Before the labeling procedure, the following preincubation step was performed—primary mouse anti-synaptotagmin1 antibody (catalog

no. 105 311, Synaptic Systems, Göttingen, Germany), diluted 1:500, and secondary anti-mouse nanobody, conjugated to superecliptic pHluorin (Custom made, NanoTag, Göttingen, Germany) diluted 1:250, were preincubated in neuronal culture medium (in 10% of the final volume for labeling) for 40 min at room temperature (RT). The preincubation ensured the formation of a stable complex between the primary antibody and the secondary nanobody. Subsequently, the labeling solution's volume was increased to the final volume required for the labeling procedure (300  $\mu$ l per coverslip). After a brief vortexing, 300  $\mu$ l of labeling solution was pipetted to the wells of a new 12-well plate (catalog no. 7696791, The Geyer, Renningen, Germany), and the coverslips containing the cultured neurons were transferred to the well plate. The cells were then incubated for 90 min at 37°C. Following incubation, the cells were washed in preheated Tyrode's solution [containing 5 mM KCl, 30 mM glucose, 124 mM NaCl, 2 mM CaCl<sub>2</sub>, 1 mM MgCl<sub>2</sub>, and 25 mM Hepes (pH 7.4)] and returned to their own conditioned media. After an additional 60 min of incubation, the neurons were ready for imaging.

### **Labeling of recycling or reserve hippocampal vesicle pools, to determine the presence of pHluorin within these pools**

Neurons were subjected to the same live-labeling procedure as described in the "Hippocampal vesicle labeling" section above. Subsequently, three distinct experiments were conducted to label different populations of synaptic vesicles. In all labeling protocols, a goat anti-VHH antibody conjugated to Alexa 647 (#128605230, Jackson ImmunoResearch Europe) was used to target specific fractions of vesicles that had been previously labeled with the synaptotagmin antibodies carrying the nanobody-pHluorin constructs.

In the first experimental paradigm, aimed to reveal all synaptic vesicles labeled with nanobody-pHluorin constructs, the cells were fixed with 4% paraformaldehyde (PFA) in phosphate-buffered saline [PBS; 10 mM Na<sub>2</sub>HPO<sub>4</sub>, 2 mM KH<sub>2</sub>PO<sub>4</sub>, 137 mM NaCl, and 2.7 mM KCl (pH 7.4)] for 20 min at RT. After fixation, the unreacted fixative groups were neutralized by application of 100 mM NH<sub>4</sub>Cl in double-distilled H<sub>2</sub>O, for 20 min at RT. The neurons were subsequently permeabilized with 0.1% Triton X-100 (#9005-64-5, Merck, Germany) in PBS, while bovine serum albumin, at 5% (#A1391-0250; Appli-chem, Germany) was used to saturate excess protein-binding sites (i.e., blocking), for 30 min. The cells were then incubated with the anti-VHH antibody (diluted 1:500 in blocking solution), for 1 hour at RT, in a custom-made humid chamber. The anti-VHH antibody recognizes the nanobody, with VHH being a synonym for nanobody. After three washes with PBS, the cells were mounted with custom-prepared Mowiol solution on a glass slide.

In the second experimental paradigm, aimed to reveal recycling vesicles, neurons were incubated in a preheated Tyrode's solution containing 50  $\mu$ M AP5 [(2R)-amino-5-phosphonopentanoate] (Tocris Bioscience, Bristol, UK; Abcam, Cambridge, UK) and 10  $\mu$ M cyanquixaline (CNQX; Tocris Bioscience, Bristol, UK; Abcam, Cambridge, UK) along with the anti-VHH antibody diluted 1:500 for 20 min at 37°C. Neurons were then stimulated for 20 s at 30 Hz, as described in the "Stimulation of rat hippocampal neurons" section. Following stimulation, the cells were fixed with 4% PFA in PBS, for 20 min, at RT, and unreacted fixative groups were neutralized, washed three times with PBS, and mounted on a glass slide, using Mowiol. AP5 and CNQX, blockers of N-methyl-D-aspartate and AMPA receptors, respectively, were used to inhibit postsynaptic responses, which could have triggered action potentials, thereby increasing the total number

of action potentials within the experiment and confusing the effects of the stimulation.

In the third experimental paradigm, designed to label surface-bound synaptotagmin 1 epitopes, neurons were live-incubated with the anti-VHH antibody, for 15 min, on ice. The cells were subsequently fixed with 4% PFA in PBS, for 20 min, on ice. After fixation, the unreacted fixative groups were neutralized, and the cells were washed three times with PBS and mounted using Mowiol.

### **Stimulation of rat hippocampal neurons**

To block recurrent activity, 50  $\mu$ M AP5 (Tocris Bioscience, Bristol, UK; Abcam, Cambridge, UK) and 10  $\mu$ M CNQX (Tocris Bioscience, Bristol, UK; Abcam, Cambridge, UK) were applied to the imaging solution (Tyrode's buffer). Electrical stimulation of the cells was carried out using field pulses at frequencies of 5, 10, 20, and 50 Hz, each lasting for 30 s at 20 mA. This stimulation was achieved with an A310 Accupulser Stimulator and a 385 Stimulus Isolator (both, World Precision Instruments, Sarasota, FL, USA), with the help of a custom-made plate field stimulator made of platinum (with a distance of 8 mm between the plates). To investigate the recruitment of vesicles from the reserve pool upon stimulation, 1  $\mu$ M baflomycin A1 (Santa Cruz Biotechnology) was added into the imaging solution. Baflomycin prevents the reacidification of vesicles following endocytic retrieval from the membrane, implying that vesicles continue to fluoresce even after recycling and thus do not induce a change in fluorescence during any subsequent round of release.

### **Imaging of vesicle release in rat hippocampal neurons**

Neurons were mounted on a custom-made live-imaging chamber filled with a prewarmed imaging solution (Tyrode's solution containing the aforementioned drugs). The cells were then imaged with an inverted Nikon Ti microscope, equipped with a Plan Apochromat 60 $\times$  1.4 numerical aperture (NA) oil objective (Nikon Corporation, Chiyoda, Tokyo, Japan), an Andor iXON 897 Electron Multiplying Charge-Coupled Device (emCCD) camera (Oxford Instruments, Andor), with a pixel size of 16  $\mu$ m  $\times$  16  $\mu$ m, Nikon D-LH Halogen 12 V 100 W Light Lamp House (Nikon Corporation, Chiyoda, Tokyo, Japan), and a cage incubator system (OKOLab, Ottaviano, Italy). Throughout the imaging procedure, a constant temperature of 37°C was maintained. The recording duration was 7 min with an imaging frequency of 1.7 frames per second and an illumination of 200 ms. The imaging protocol was executed as follows: After an initial 30-s baseline, the cells were stimulated for 30 s, followed by a 30-s recovery period. This stimulation-recovery cycle was repeated four times in total, with an increasing frequency (5, 10, 20, and 50 Hz). Subsequently, there was a 120-s recovery period followed by the addition of 100 mM NH<sub>4</sub>Cl (fig. S4A). NH<sub>4</sub>Cl is applied to alkalinize the pH within all synaptic vesicles and thus to reveal all pHluorin signals. pHluorin is in a dark state at the low pH inside synaptic vesicles; NH<sub>4</sub>Cl addition raises the pH and enables pHluorin to emit photons.

For the experiments described in the "Labeling of recycling or reserve hippocampal vesicle pools, to determine the presence of pHluorin within these pools" section, all three conditions were imaged at a Nikon Eclipse Ti microscope equipped with a plan apochromat 60 $\times$  1.4 NA oil-immersion objective lens, DS-Qi2 complementary metal-oxide semiconductor camera with a pixel size of

7.3  $\mu\text{m} \times 7.3 \mu\text{m}$ , and a Nikon halogen lamp (Nikon Corporation, Chiyoda, Tokyo, Japan).

### Image analysis of rat hippocampal neuron data

Synapses were identified automatically, using band-a-pass filter procedure to reveal suitably sized spots, followed by an automated thresholding approach, which removed noise spots (using MATLAB version R2022b, The MathWorks Inc.). This procedure was applied on a summed image, produced by adding all movie frames into one image, and identified many regions of interest (ROIs) for each movie. The signal within all ROIs was then recorded and was normalized by the initial baseline signal (before the first stimulation round). The peak amplitude was measured for each stimulation round (fig. S4B).

The data in Fig. 5D were computed as follows: The peak pHluorin signals corresponding to the respective stimuli, representing the vesicle pools released by each stimulus, were normalized to the signal provided by the NH<sub>4</sub>Cl application, which represents the entire labeled vesicle population, since this application alkalinizes the pH inside all vesicles. The values were then combined and plotted. For the bafilomycin treatment, the peak value represents the plateau value reached before the next stimulus.

For the experiments described in the “Labeling of recycling or reserve hippocampal vesicle pools, to determine the presence of pHluorin within these pools” section, all images were analyzed using self-written macros developed in MATLAB (The Mathworks Inc., Natick, MA, USA; version R2023a). Total intensity values were obtained by summing the pixel intensities in a selected region, in each image. These intensity values were then corrected for background, used for statistical analysis, and performed with GraphPad Prism (Prism 10, version 10.3.0, GraphPad Software LLC). For the statistical analysis, the data were tested for normality using the Shapiro-Wilk test and were subsequently analyzed with the Kruskal-Wallis test, followed by Dunn’s multiple comparisons test for post hoc analysis.

### Supplementary Materials

The PDF file includes:

Figs. S1 to S7

Tables S1 to S4

Legends for movies S1 to S3

References

Other Supplementary Material for this manuscript includes the following:

Movies S1 to S3

### REFERENCES AND NOTES

- T. C. Südhof, Calcium control of neurotransmitter release. *Cold Spring Harb. Perspect. Biol.* **4**, a011353 (2012).
- A. T. Brunger, U. B. Choi, Y. Lai, J. Leitz, Q. J. Zhou, Molecular mechanisms of fast neurotransmitter release, in *Annual Review of Biophysics*, Vol 47, K. A. Dill, Ed. (Annual Review of Biophysics, Annual Reviews, 2018), vol. 47, pp. 469–497.
- C. Acuna, X. Liu, T. C. Südhof, How to make an active zone: Unexpected universal functional redundancy between RIMs and RIM-BPs. *Neuron* **91**, 792–807 (2016).
- T. C. Südhof, The molecular machinery of neurotransmitter release (Nobel Lecture). *Angew. Chem. Int. Ed. Engl.* **53**, 12696–12717 (2014).
- T. C. Südhof, Neurotransmitter release: The last millisecond in the life of a synaptic vesicle. *Neuron* **80**, 675–690 (2013).
- S. O. Rizzoli, W. J. Betz, The structural organization of the readily releasable pool of synaptic vesicles. *Science* **303**, 2037–2039 (2004).
- C. Rosenmund, C. F. Stevens, Definition of the readily releasable pool of vesicles at hippocampal synapses. *Neuron* **16**, 1197–1207 (1996).
- S. O. Rizzoli, W. J. Betz, Synaptic vesicle pools. *Nat. Rev. Neurosci.* **6**, 57–69 (2005).
- A. Denker, S. O. Rizzoli, Synaptic vesicle pools: An update. *Front. Synaptic Neurosci.* **2**, 135 (2010).
- S. Chamberland, K. Tóth, Functionally heterogeneous synaptic vesicle pools support diverse synaptic signalling. *J. Physiol.* **594**, 825–835 (2016).
- N. Harata, J. L. Pyle, A. M. Aravanis, M. Mozhayeva, E. T. Kavalali, R. W. Tsien, Limited numbers of recycling vesicles in small CNS nerve terminals: Implications for neural signaling and vesicular cycling. *Trends Neurosci.* **24**, 637–643 (2001).
- F. Opazo, S. O. Rizzoli, Studying synaptic vesicle pools using photoconversion of styryl dyes. *J. Vis. Exp.*, e1790 (2010).
- N. Harata, T. A. Ryan, S. J. Smith, J. Buchanan, R. W. Tsien, Visualizing recycling synaptic vesicles in hippocampal neurons by FM 1-43 photoconversion. *Proc. Natl. Acad. Sci. U.S.A.* **98**, 12748–12753 (2001).
- T. Schikorski, C. F. Stevens, Morphological correlates of functionally defined synaptic vesicle populations. *Nat. Neurosci.* **4**, 391–395 (2001).
- Y. Hua, R. Sinha, C. S. Thiel, R. Schmidt, J. Hüve, H. Martens, S. W. Hell, A. Egner, J. Klingauf, A readily retrievable pool of synaptic vesicles. *Nat. Neurosci.* **14**, 833–839 (2011).
- S. Krishnan, J. Klingauf, The readily retrievable pool of synaptic vesicles. *Biol. Chem.* **404**, 385–397 (2023).
- K. Ikeda, J. M. Bekkers, Counting the number of releasable synaptic vesicles in a presynaptic terminal. *Proc. Natl. Acad. Sci. U.S.A.* **106**, 2945–2950 (2009).
- B. G. Wilhelm, S. Mandad, S. Truckenbrodt, K. Kröhnert, C. Schäfer, B. Rammner, S. J. Koo, G. A. Claßen, M. Krauss, V. Haucke, H. Urlaub, S. O. Rizzoli, Composition of isolated synaptic boutons reveals the amounts of vesicle trafficking proteins. *Science* **344**, 1023–1028 (2014).
- F. Schweizer, T. Ryan, The synaptic vesicle: Cycle of exocytosis and endocytosis. *Curr. Opin. Neurobiol.* **16**, 298–304 (2006).
- S. Hilfiker, V. A. Pieribone, A. J. Czernik, H. T. Kao, G. J. Augustine, P. Greengard, Synapsins as regulators of neurotransmitter release. *Philos. Trans. R. Soc. Lond. B Biol. Sci.* **354**, 269–279 (1999).
- A. Orenbuch, L. Shalev, V. Marra, I. Sinai, Y. Levy, J. Kahn, J. J. Burden, K. Staras, D. Gitler, Synapsin selectively controls the mobility of resting pool vesicles at hippocampal terminals. *J. Neurosci.* **32**, 3969–3980 (2012).
- A. Peichstein, N. Tomilin, K. Fredrich, O. Vorontsova, E. Sopova, E. Evergren, V. Haucke, L. Brodin, O. Shupliakov, Vesicle clustering in a living synapse depends on a synapsin region that mediates phase separation. *Cell Rep.* **30**, 2594–2602.e3 (2020).
- S. Reshetniak, S. O. Rizzoli, The vesicle cluster as a major organizer of synaptic composition in the short-term and long-term. *Curr. Opin. Cell Biol.* **71**, 63–68 (2021).
- N. Hirokawa, K. Sobue, K. Kanda, A. Harada, H. Yorifuji, The cytoskeletal architecture of the presynaptic terminal and molecular structure of synapsin 1. *J. Cell Biol.* **108**, 111–126 (1989).
- D. Kamin, M. A. Lauterbach, V. Westphal, J. Keller, A. Schönle, S. W. Hell, S. O. Rizzoli, High- and low-mobility stages in the synaptic vesicle cycle. *Biophys. J.* **99**, 675–684 (2010).
- S. Truckenbrodt, A. Viplav, S. Jähne, A. Vogts, A. Denker, H. Wildhagen, E. F. Fornasiero, S. O. Rizzoli, Newly produced synaptic vesicle proteins are preferentially used in synaptic transmission. *EMBO J.* **37**, e98044 (2018).
- F. Cesca, P. Baldelli, F. Valtorta, F. Benfenati, The synapsins: Key actors of synapse function and plasticity. *Prog. Neurobiol.* **91**, 313–348 (2010).
- N. Chenouard, F. Xuan, R. W. Tsien, Synaptic vesicle traffic is supported by transient actin filaments and regulated by PKA and NO. *Nat. Commun.* **11**, 5318 (2020).
- A. Pernia-Andrade, P. Jonas, The multiple faces of RIM. *Neuron* **69**, 185–187 (2011).
- V. A. Cazares, M. M. Njus, A. Manly, J. J. Saldate, A. Subramani, Y. Ben-Simon, M. A. Sutton, U. Ashery, E. L. Stuenkel, Dynamic partitioning of synaptic vesicle pools by the SNARE-binding protein tomosyn. *J. Neurosci.* **36**, 11208–11222 (2016).
- F. C. Guarnieri, How do synaptic vesicles “know” which pool they belong to? *J. Neurosci.* **37**, 2276–2278 (2017).
- S. H. Kim, T. A. Ryan, CDK5 serves as a major control point in neurotransmitter release. *Neuron* **67**, 797–809 (2010).
- A. R. Gallimore, A. R. Aricescu, M. Yuzaki, R. Calinescu, A computational model for the AMPA receptor phosphorylation master switch regulating cerebellar long-term depression. *PLOS Comput. Biol.* **12**, e1004664 (2016).
- A. R. Gallimore, T. Kim, K. Tanaka-Yamamoto, E. De Schutter, Switching on depression and potentiation in the cerebellum. *Cell Rep.* **22**, 722–733 (2018).
- G. Antunes, E. De Schutter, A stochastic signaling network mediates the probabilistic induction of cerebellar long-term depression. *J. Neurosci.* **32**, 9288–9300 (2012).
- T. Mäki-Marttunen, N. Iannella, A. G. Edwards, G. T. Einevoll, K. T. Blackwell, A unified computational model for cortical post-synaptic plasticity. *eLife* **9**, e55714 (2020).
- K. T. Blackwell, J. Jedrzejewska-Szmk, Molecular mechanisms underlying neuronal synaptic plasticity: Systems biology meets computational neuroscience in the wilds of synaptic plasticity. *Wiley Interdiscip. Rev. Syst. Biol. Med.* **5**, 717–731 (2013).

38. Y. Kitagawa, T. Hirano, S.-y. Kawaguchi, Prediction and validation of a mechanism to control the threshold for inhibitory synaptic plasticity. *Mol. Syst. Biol.* **5**, 280 (2009).
39. U. S. Bhalla, R. Iyengar, Emergent properties of networks of biological signaling pathways. *Science* **283**, 381–387 (1999).
40. I. Hepburn, A. Jain, H. Gangal, Y. Yamamoto, K. Tanaka-Yamamoto, E. De Schutter, A model of induction of cerebellar long-term depression including RKIP inactivation of Raf and MEK. *Front. Mol. Neurosci.* **10**, 19 (2017).
41. F. Luo, M. Dittrich, S. Cho, J. R. Stiles, S. D. Meriney, Transmitter release is evoked with low probability predominately by calcium flux through single channel openings at the frog neuromuscular junction. *J. Neurophysiol.* **113**, 2480–2489 (2015).
42. M. Dittrich, J. M. Pattillo, J. D. King, S. Cho, J. R. Stiles, S. D. Meriney, An excess-calcium-binding-site model predicts neurotransmitter release at the neuromuscular junction. *Biophys. J.* **104**, 2751–2763 (2013).
43. I. Hepburn, W. Chen, S. Wils, E. De Schutter, STEPS: Efficient simulation of stochastic reaction-diffusion models in realistic morphologies. *BMC Syst. Biol.* **6**, 36 (2012).
44. W. Chen, E. De Schutter, Parallel STEPS: Large scale stochastic spatial reaction-diffusion simulation with high performance computers. *Front. Neuroinform.* **11**, 13 (2017).
45. J. J. Tapia, A. S. Saglam, J. Czech, R. Kuczewski, T. M. Bartol, T. J. Sejnowski, J. R. Faeder, MCCell-R: A particle-resolution network-free spatial modeling framework. *Methods Mol. Biol.* **1945**, 203–229 (2019).
46. I. Hepburn, J. Lallouette, W. Chen, A. R. Gallimore, S. Y. Nagasawa-Soeda, E. De Schutter, Vesicle and reaction-diffusion hybrid modeling with STEPS. *Commun. Biol.* **7**, 573 (2024).
47. S. Reshetniak, J. E. Ußling, E. Perego, B. Rammner, T. Schikorski, E. F. Fornasiero, S. Truckenbrodt, S. Köster, S. O. Rizzoli, A comparative analysis of the mobility of 45 proteins in the synaptic bouton. *EMBO J.* **39**, e104596 (2020).
48. D. Milovanovic, P. De Camilli, Synaptic vesicle clusters at synapses: A distinct liquid phase? *Neuron* **93**, 995–1002 (2017).
49. D. Milovanovic, Y. Wu, X. Bian, P. De Camilli, A liquid phase of synapsin and lipid vesicles. *Science* **361**, 604–607 (2018).
50. J. Waters, S. J. Smith, Vesicle pool partitioning influences presynaptic diversity and weighting in rat hippocampal synapses. *J. Physiol.* **541**, 811–823 (2002).
51. T. Nakashiba, J. Z. Young, T. J. McHugh, D. L. Buhl, S. Tonegawa, Transgenic inhibition of synaptic transmission reveals role of CA3 output in hippocampal learning. *Science* **319**, 1260–1264 (2008).
52. T. Fernández-Alfonso, T. A. Ryan, The kinetics of synaptic vesicle pool depletion at CNS synaptic terminals. *Neuron* **41**, 943–953 (2004).
53. J. Balaji, T. A. Ryan, Single-vesicle imaging reveals that synaptic vesicle exocytosis and endocytosis are coupled by a single stochastic mode. *Proc. Natl. Acad. Sci. U.S.A.* **104**, 20576–20581 (2007).
54. M. Armbruster, M. Messa, S. M. Ferguson, P. De Camilli, T. A. Ryan, Dynamin phosphorylation controls optimization of endocytosis for brief action potential bursts. *eLife* **2**, e00845 (2013).
55. J. E. Hassinger, G. Oster, D. G. Drubin, P. Rangamani, Design principles for robust vesiculation in clathrin-mediated endocytosis. *Proc. Natl. Acad. Sci. U.S.A.* **114**, E1118–E1127 (2017).
56. T. A. Ryan, S. J. Smith, Vesicle pool mobilization during action-potential firing at hippocampal synapses. *Neuron* **14**, 983–989 (1995).
57. T. Yoshimori, A. Yamamoto, Y. Moriyama, M. Futai, Y. Tashiro, Bafilomycin A1, a specific inhibitor of vacuolar-type H<sup>+</sup>-ATPase, inhibits acidification and protein degradation in lysosomes of cultured cells. *J. Biol. Chem.* **266**, 17707–17712 (1991).
58. S. M. Sertel, W. Blumenstein, S. Mandad, O. Shomroni, G. Salinas, S. O. Rizzoli, Differences in synaptic vesicle pool behavior between male and female hippocampal cultured neurons. *Sci. Rep.* **11**, 17374 (2021).
59. B. G. Wilhelm, T. W. Groemer, S. O. Rizzoli, The same synaptic vesicles drive active and spontaneous release. *Nat. Neurosci.* **13**, 1454–1456 (2010).
60. M. A. Gaffield, S. O. Rizzoli, W. J. Betz, Mobility of synaptic vesicles in different pools in resting and stimulated frog motor nerve terminals. *Neuron* **51**, 317–325 (2006).
61. R. Fernández-Busná Diego, B. Zuber, U. E. Maurer, M. Cyrklaff, W. Baumeister, V. Lucic, Quantitative analysis of the native presynaptic cytomatrix by cryoelectron tomography. *J. Cell Biol.* **188**, 145–156 (2010).
62. T. Wöllert, A. Patel, Y.-L. Lee, D. W. Provance, V. E. Vought, M. S. Cosgrove, J. A. Mercer, G. M. Langford, Myosin5a tail associates directly with Rab3A-containing compartments in neurons. *J. Biol. Chem.* **286**, 14352–14361 (2011).
63. L. G. Dolce, N. Ohbayashi, D. F. C. da Silva, A. J. R. Ferrari, R. A. S. Pirolla, A. C. d. A. P. Schwarzer, L. M. Zanphorlin, L. Cabral, M. Fioramonte, C. H. I. Ramos, F. C. Gozzo, M. Fukuda, P. O. Giuseppe, M. T. Murakami, Unveiling the interaction between the molecular motor Myosin Vc and the small GTPase Rab3A. *J. Proteomics* **212**, 103549 (2020).
64. A. J. Lindsay, F. Jollivet, C. P. Horgan, A. R. Khan, G. Raposo, M. W. McCaffrey, B. Goud, Identification and characterization of multiple novel Rab-myosin Va interactions. *Mol. Biol. Cell* **24**, 3420–3434 (2013).
65. D. Maschi, M. W. Gramlich, V. A. Klyachko, Myosin V functions as a vesicle tether at the plasma membrane to control neurotransmitter release in central synapses. *eLife* **7**, e39440 (2018).
66. A. Denker, I. Bethani, K. Kröhnert, C. Körber, H. Horstmann, B. G. Wilhelm, S. V. Barysch, T. Kuner, E. Neher, S. O. Rizzoli, A small pool of vesicles maintains synaptic activity in vivo. *Proc. Natl. Acad. Sci. U.S.A.* **108**, 17177–17182 (2011).
67. T. Kögel, H. H. Gerdes, Roles of myosin Va and Rab3D in membrane remodeling of immature secretory granules. *Cell. Mol. Neurobiol.* **30**, 1303–1308 (2010).
68. H. Taschenberger, A. Woehler, E. Neher, Superpriming of synaptic vesicles as a common basis for intersynapse variability and modulation of synaptic strength. *Proc. Natl. Acad. Sci. U.S.A.* **113**, E4548–E4557 (2016).
69. J. M. McEwen, J. M. Madison, M. Dybbs, J. M. Kaplan, Antagonistic regulation of synaptic vesicle priming by Tomosyn and UNC-13. *Neuron* **51**, 303–315 (2006).
70. S. Park, N.-R. Bin, B. Yu, R. Wong, E. Sitaras, K. Sugita, K. Ma, J. Xu, C.-W. Tien, A. Algouneh, E. Turlova, S. Wang, P. Siruya, W. Shahid, L. Kalia, Z. P. Feng, P. P. Monnier, H.-S. Sun, M. Zhen, S. Gao, J. Rizo, S. Sugita, UNC-18 and Tomosyn antagonistically control synaptic vesicle priming downstream of UNC-13 in *Caenorhabditis elegans*. *J. Neurosci.* **37**, 8797–8815 (2017).
71. U. Ashery, N. Bielopolski, B. Barak, O. Yizhar, Friends and foes in synaptic transmission: The role of tomosyn in vesicle priming. *Trends Neurosci.* **32**, 275–282 (2009).
72. Y. Yamamoto, S. Mochida, T. Kurooka, T. Sakisaka, Reciprocal intramolecular interactions of tomosyn control its inhibitory activity on SNARE complex formation. *J. Biol. Chem.* **284**, 12480–12490 (2009).
73. Y. Yamamoto, K. Fujikura, M. Sakaue, K. Okimura, Y. Kobayashi, T. Nakamura, T. Sakisaka, The tail domain of tomosyn controls membrane fusion through tomosyn displacement by VAMP2. *Biochem. Biophys. Res. Commun.* **399**, 24–30 (2010).
74. S. O. Rizzoli, R. Jahn, Kiss-and-run, collapse and ‘readily retrievable’ vesicles. *Traffic* **8**, 1137–1144 (2007).
75. C. F. Stevens, J. H. Williams, “Kiss and run” exocytosis at hippocampal synapses. *Proc. Natl. Acad. Sci. U.S.A.* **97**, 12828–12833 (2000).
76. E. M. Wenzel, A. Morton, K. Ebert, O. Welzel, J. Kornhuber, M. A. Cousin, T. W. Groemer, Key physiological parameters dictate triggering of activity-dependent bulk endocytosis in hippocampal synapses. *PLOS ONE* **7**, e38188 (2012).
77. T. H. Nguyen, X. Qiu, J. Sun, F. A. Meunier, Bulk endocytosis at neuronal synapses. *Sci. China Life Sci.* **57**, 378–383 (2014).
78. W. Chen, I. Hepburn, A. Martyushev, E. De Schutter, Modeling neurons in 3D at the nanoscale. *Adv. Exp. Med. Biol.* **1359**, 3–24 (2022).
79. A. Denker, K. Kröhnert, J. Bückers, E. Neher, S. O. Rizzoli, The reserve pool of synaptic vesicles acts as a buffer for proteins involved in synaptic vesicle recycling. *Proc. Natl. Acad. Sci. U.S.A.* **108**, 17183–17188 (2011).
80. S. Takamori, M. Holt, K. Stenius, E. A. Lemke, M. Gronborg, D. Riedel, H. Urlaub, S. Schenck, B. Brügger, P. Ringler, S. A. Müller, B. Rammner, F. Gräter, J. S. Hub, B. L. De Groot, G. Mieskes, Y. Moriyama, J. Klingauf, H. Grubmüller, J. Heuser, F. Wieland, R. Jahn, Molecular anatomy of a trafficking organelle. *Cell* **127**, 831–846 (2006).
81. S. A. Rey, C. A. Smith, M. W. Fowler, F. Crawford, J. J. Burden, K. Staras, Ultrastructural and functional fate of recycled vesicles in hippocampal synapses. *Nat. Commun.* **6**, 8043 (2015).
82. J. Roos, R. B. Kelly, The endocytic machinery in nerve terminals surrounds sites of exocytosis. *Curr. Biol.* **9**, 1411–1414 (1999).
83. T. Schikorski, C. F. Stevens, Quantitative ultrastructural analysis of hippocampal excitatory synapses. *J. Neurosci.* **17**, 5858–5867 (1997).
84. I. Dululova, X. Lou, J. Lu, I. Huryeva, A. Alam, R. Schneeggenburger, T. C. Südhof, J. Rizo, A Munc13/RIM/Rab3 tripartite complex: From priming to plasticity? *EMBO J.* **24**, 2839–2850 (2005).
85. L. Deng, P. S. Kaeser, W. Xu, T. C. Südhof, RIM proteins activate vesicle priming by reversing autoinhibitory homodimerization of Munc13. *Neuron* **69**, 317–331 (2011).
86. M. Camacho, J. Basu, T. Trimbuch, S. Chang, C. Pulido-Lozano, S. S. Chang, I. Dululova, M. Abo-Rady, J. Rizo, C. Rosenmund, Heterodimerization of Munc13 C. *Nat. Commun.* **8**, 15293 (2017).
87. J. Lu, M. Machiusi, I. Dululova, H. Dai, T. C. Südhof, D. R. Tomchick, J. Rizo, Structural basis for a Munc13-1 homodimer to Munc13-1/RIM heterodimer switch. *PLOS Biol.* **4**, e192 (2006).
88. C. Imig, S.-W. Min, S. Krinner, M. Arancillo, C. Rosenmund, T. C. Südhof, J. Rhee, N. Brose, B. H. Cooper, The morphological and molecular nature of synaptic vesicle priming at presynaptic active zones. *Neuron* **84**, 416–431 (2014).
89. V. N. Murthy, C. F. Stevens, Reversal of synaptic vesicle docking at central synapses. *Nat. Neurosci.* **2**, 503–507 (1999).
90. N. E. Ziv, Maintaining the active zone: Demand, supply and disposal of core active zone proteins. *Neurosci. Res.* **127**, 70–77 (2018).
91. H. Anwar, I. Hepburn, H. Nedelescu, W. L. Chen, E. De Schutter, Stochastic calcium mechanisms cause dendritic calcium spike variability. *J. Neurosci.* **33**, 15848–15867 (2013).

92. D. Althof, D. Baehrens, M. Watanabe, N. Suzuki, B. Fakler, Á. Kulik, Inhibitory and excitatory axon terminals share a common nano-architecture of their  $\text{Ca}_{v}2.1$  (P/Q-type)  $\text{Ca}^{2+}$  channels. *Front. Cell. Neurosci.* **9**, 315 (2015).
93. D. Zenisek, J. A. Steyer, W. Almers, Transport, capture and exocytosis of single synaptic vesicles at active zones. *Nature* **406**, 849–854 (2000).
94. C. Ma, W. Li, Y. Xu, J. Rizo, Munc13 mediates the transition from the closed syntaxin-Munc18 complex to the SNARE complex. *Nat. Struct. Mol. Biol.* **18**, 542–549 (2011).
95. C. Ma, L. Su, A. B. Seven, Y. Xu, J. Rizo, Reconstitution of the vital functions of Munc18 and Munc13 in neurotransmitter release. *Science* **339**, 421–425 (2013).
96. T. Shu, H. Jin, J. E. Rothman, Y. Zhang, Munc13-1 MUN domain and Munc18-1 cooperatively chaperone SNARE assembly through a tetrameric complex. *Proc. Natl. Acad. Sci. U.S.A.* **117**, 1036–1041 (2020).
97. D. Zikich, A. Mezer, F. Varoqueaux, A. Sheinin, H. J. Junge, E. Nachliel, R. Melamed, N. Brose, M. Gutman, U. Ashery, Vesicle priming and recruitment by ubMunc13-2 are differentially regulated by calcium and calmodulin. *J. Neurosci.* **28**, 1949–1960 (2008).
98. Y. Lai, J. J. Diao, D. J. Cipriano, Y. X. Zhang, R. A. Pfuetzner, M. S. Padolina, A. T. Brunger, Complexin inhibits spontaneous release and synchronizes  $\text{Ca}^{2+}$ -triggered synaptic vesicle fusion by distinct mechanisms. *eLife* **3**, e03756 (2014).
99. Y. Lai, U. B. Choi, J. Leitz, H. J. Rhee, C. Lee, B. Altas, M. L. Zhao, R. A. Pfuetzner, A. L. Wang, N. Brose, J. Rhee, A. T. Brunger, Molecular mechanisms of synaptic vesicle priming by Munc13 and Munc18. *Neuron* **95**, 591–607.e10 (2017).
100. A. F. Davis, J. Bai, D. Fasshauer, M. J. Wolowick, J. L. Lewis, E. R. Chapman, Kinetics of synaptotagmin responses to  $\text{Ca}^{2+}$  and assembly with the core SNARE complex onto membranes. *Neuron* **24**, 363–376 (1999).
101. E. Hui, J. Bai, P. Wang, M. Sugimori, R. R. Llinas, E. R. Chapman, Three distinct kinetic groupings of the synaptotagmin family: Candidate sensors for rapid and delayed exocytosis. *Proc. Natl. Acad. Sci. U.S.A.* **102**, 5210–5214 (2005).
102. C. Rosenmund, J. D. Clements, G. L. Westbrook, Nonuniform probability of glutamate release at a hippocampal synapse. *Science* **262**, 754–757 (1993).
103. V. N. Murthy, T. J. Sejnowski, C. F. Stevens, Heterogeneous release properties of visualized individual hippocampal synapses. *Neuron* **18**, 599–612 (1997).
104. T. Branco, K. Staras, PERSPECTIVES The probability of neurotransmitter release: Variability and feedback control at single synapses. *Nat. Rev. Neurosci.* **10**, 373–383 (2009).
105. J. S. Dittman, T. A. Ryan, The control of release probability at nerve terminals. *Nat. Rev. Neurosci.* **20**, 177–186 (2019).
106. Y. Nakamura, H. Harada, N. Kamasawa, K. Matsui, J. S. Rothman, R. Shigemoto, R. A. Silver, D. A. DiGregorio, T. Takahashi, Nanoscale distribution of presynaptic  $\text{Ca}^{2+}$  channels and its impact on vesicular release during development. *Neuron* **85**, 145–158 (2015).
107. M. Armbruster, T. A. Ryan, Synaptic vesicle retrieval time is a cell-wide rather than individual-synapse property. *Nat. Neurosci.* **14**, 824–826 (2011).
108. P. Atluri, T. Ryan, The kinetics of synaptic vesicle reacidification at hippocampal nerve terminals. *J. Neurosci.* **26**, 2313–2320 (2006).
109. T. Hori, T. Takahashi, Kinetics of synaptic vesicle refilling with neurotransmitter glutamate. *Neuron* **76**, 511–517 (2012).
110. P. Chi, P. Greengard, T. A. Ryan, Synapsin dispersion and reclustering during synaptic activity. *Nat. Neurosci.* **4**, 1187–1193 (2001).
111. N. Gimber, G. Tadeus, T. Maritzen, J. Schmoranzer, V. Haucke, Diffusional spread and confinement of newly exocytosed synaptic vesicle proteins. *Nat. Commun.* **6**, 8392 (2015).
112. V. Haucke, E. Neher, S. J. Sigrist, Protein scaffolds in the coupling of synaptic exocytosis and endocytosis. *Nat. Rev. Neurosci.* **12**, 127–138 (2011).
113. M. Zhao, S. Wu, Q. Zhou, S. Vivona, D. J. Cipriano, Y. Cheng, A. T. Brunger, Mechanistic insights into the recycling machine of the SNARE complex. *Nature* **518**, 61–67 (2015).
114. S. Vivona, D. J. Cipriano, S. O’Leary, Y. H. Li, T. D. Fenn, A. T. Brunger, Disassembly of all SNARE complexes by N-ethylmaleimide-sensitive factor (NSF) is initiated by a conserved 1:1 interaction between  $\alpha$ -soluble NSF attachment protein (SNAP) and SNARE complex. *J. Biol. Chem.* **288**, 24984–24991 (2013).
115. D. J. Cipriano, J. Jung, S. Vivona, T. D. Fenn, A. T. Brunger, Z. Bryant, Processive ATP-driven substrate disassembly by the N-ethylmaleimide-sensitive factor (NSF) molecular machine. *J. Biol. Chem.* **288**, 23436–23445 (2013).
116. F. Benfenati, F. Valtorta, M. C. Rossi, F. Onofri, T. Sihra, P. Greengard, Interactions of synapsin I with phospholipids: Possible role in synaptic vesicle clustering and in the maintenance of bilayer structures. *J. Cell Biol.* **123**, 1845–1855 (1993).
117. J. J. Cheetham, T. Helfiker, F. Benfenati, T. Weber, P. Greengard, A. J. Czernik, Identification of synapsin I peptides that insert into lipid membranes. *Biochem. J.* **354**, 57–66 (2001).
118. M. Hosaka, R. E. Hammer, T. C. Südhof, A phospho-switch controls the dynamic association of synapsins with synaptic vesicles. *Neuron* **24**, 377–387 (1999).
119. G. Stefani, F. Onofri, F. Valtorta, P. Vaccaro, P. Greengard, F. Benfenati, Kinetic analysis of the phosphorylation-dependent interactions of synapsin I with rat brain synaptic vesicles. *J. Physiol.* **504**, 501–515 (1997).
120. G. A. Banker, W. M. Cowan, Rat hippocampal neurons in dispersed cell culture. *Brain Res.* **126**, 397–425 (1977).
121. S. Kaech, G. Bunker, Culturing hippocampal neurons. *Nat. Protoc.* **1**, 2406–2415 (2006).
122. V. Anggono, K. J. Smillie, M. E. Graham, V. A. Valova, M. A. Cousin, P. J. Robinson, Syndapin I is the phosphorylation-regulated dynamin I partner in synaptic vesicle endocytosis. *Nat. Neurosci.* **9**, 752–760 (2006).
123. B. Barak, A. Williams, N. Bielopolski, I. Gottfried, E. Okun, M. A. Brown, U. Matti, J. Rettig, E. L. Stuenkel, U. Ashery, Tomosyn expression pattern in the mouse hippocampus suggests both presynaptic and postsynaptic functions. *Front. Neuroanat.* **4**, 149 (2010).
124. T. M. Bartol, D. X. Keller, J. P. Kinney, C. L. Bajaj, K. M. Harris, T. J. Sejnowski, M. B. Kennedy, Computational reconstitution of spine calcium transients from individual proteins. *Front. Synaptic Neurosci.* **7**, 17 (2015).
125. M. E. Bowen, K. Weninger, J. Ernst, S. Chu, A. T. Brunger, Single-molecule studies of synaptotagmin and complexin binding to the SNARE complex. *Biophys. J.* **89**, 690–702 (2005).
126. P. Burkhardt, D. A. Hattendorf, W. I. Weis, D. Fasshauer, Munc18a controls SNARE assembly through its interaction with the syntaxin N-peptide. *EMBO J.* **27**, 923–933 (2008).
127. J. D. Buxbaum, Y. Dudai, A quantitative model for the kinetics of cAMP-dependent protein kinase (type II) activity. Long-term activation of the kinase and its possible relevance to learning and memory. *J. Biol. Chem.* **264**, 9344–9351 (1989).
128. J. Chugh, A. Chatterjee, A. Kumar, R. K. Mishra, R. Mittal, R. V. Hosur, Structural characterization of the large soluble oligomers of the GTPase effector domain of dynamin. *FEBS J.* **273**, 388–397 (2006).
129. T. Coppola, S. Magnin-Luthi, V. Perret-Menoud, S. Gattesco, G. Schiavo, R. Regazzi, Direct interaction of the Rab3 effector RIM with  $\text{Ca}^{2+}$  channels, SNAP-25, and synaptotagmin. *J. Biol. Chem.* **276**, 32756–32762 (2001).
130. M. K. Diril, M. Wienisch, N. Jung, J. Klingauf, V. Haucke, Stonin 2 is an AP-2-dependent endocytic sorting adaptor for synaptotagmin internalization and recycling. *Dev. Cell* **10**, 233–244 (2006).
131. T. Doi, S. Kuroda, T. Michikawa, M. Kawato, Inositol 1,4,5-trisphosphate-dependent  $\text{Ca}^{2+}$  threshold dynamics detect spike timing in cerebellar Purkinje cells. *J. Neurosci.* **25**, 950–961 (2005).
132. G. C. Faas, S. Raghavachari, J. E. Lisman, I. Mody, Calmodulin as a direct detector of  $\text{Ca}^{2+}$  signals. *Nat. Neurosci.* **14**, 301–304 (2011).
133. G. C. Faas, B. Schwaller, J. L. Vergara, I. Mody, Resolving the fast kinetics of cooperative binding:  $\text{Ca}^{2+}$  buffering by calretinin. *PLoS Biol.* **5**, e311 (2007).
134. Y. Fujita, H. Shirataki, T. Sakisaka, T. Asakura, T. Ohya, H. Kotani, S. Yokoyama, H. Nishioka, Y. Matsuura, A. Mizoguchi, R. H. Scheller, Y. Takai, Tomosyn: A syntaxin-1-binding protein that forms a novel complex in the neurotransmitter release process. *Neuron* **20**, 905–915 (1998).
135. S. L. Gordon, M. A. Cousin, The Sybtraps: Control of synaptobrevin traffic by synaptophysin,  $\alpha$ -synuclein and AP-180. *Traffic* **15**, 245–254 (2014).
136. H. C. Hemmings Jr., A. C. Nairn, P. Greengard, DARPP-32, a dopamine- and adenosine 3’:5’-monophosphate-regulated neuronal phosphoprotein. II. Comparison of the kinetics of phosphorylation of DARPP-32 and phosphatase inhibitor 1. *J. Biol. Chem.* **259**, 14491–14497 (1984).
137. J. R. Jimah, J. E. Hinshaw, Structural insights into the mechanism of dynamin superfamily proteins. *Trends Cell Biol.* **29**, 257–273 (2019).
138. S. Kawaguchi, T. Hirano, Gating of long-term depression by  $\text{Ca}^{2+}$ /calmodulin-dependent protein kinases through enhanced cGMP signalling in cerebellar Purkinje cells. *J. Physiol.* **591**, 1707–1730 (2013).
139. M. M. King, C. Y. Huang, P. B. Chock, A. C. Nairn, H. C. Hemmings Jr., K. F. Chan, P. Greengard, Mammalian brain phosphoproteins as substrates for calcineurin. *J. Biol. Chem.* **259**, 8080–8083 (1984).
140. Y. L. Li, G. J. Augustine, K. Weninger, Kinetics of complexin binding to the SNARE complex: Correcting single molecule FRET measurements for hidden events. *Biophys. J.* **93**, 2178–2187 (2007).
141. M. Liu, E. Girma, M. A. Glicksman, R. L. Stein, Kinetic mechanistic studies of Cdk5/p25-catalyzed H1P phosphorylation: Metal effect and solvent kinetic isotope effect. *Biochemistry* **49**, 4921–4929 (2010).
142. M. Liu, S. Choi, G. D. Cuny, K. Ding, B. C. Dobson, M. A. Glicksman, K. Auerbach, R. L. Stein, Kinetic studies of Cdk5/p25 kinase: Phosphorylation of tau and complex inhibition by two prototype inhibitors. *Biochemistry* **47**, 8367–8377 (2008).
143. A. Mezer, E. Nachliel, M. Gutman, U. Ashery, A new platform to study the molecular mechanisms of exocytosis. *J. Neurosci.* **24**, 8838–8846 (2004).
144. O. Millet, P. Bernadó, J. García, J. Rizo, M. Pons, NMR measurement of the off rate from the first calcium-binding site of the synaptotagmin I C2A domain. *FEBS Lett.* **516**, 93–96 (2002).
145. C. Rickman, B. Davletov, Mechanism of calcium-independent synaptotagmin binding to target SNAREs. *J. Biol. Chem.* **278**, 5501–5504 (2003).
146. J. A. Ross, M. A. Digman, L. Wang, E. Gratton, J. P. Albanesi, D. M. Jameson, Oligomerization state of dynamin 2 in cell membranes using TIRF and number and brightness analysis. *Biophys. J.* **100**, L15–L17 (2011).
147. B. N. Shin, D. W. Kim, I. H. Kim, J. H. Park, J. H. Ahn, I. J. Kang, Y. L. Lee, C.-H. Lee, I. K. Hwang, Y.-M. Kim, S. Ryoo, T.-K. Lee, M.-H. Won, J.-C. Lee, Down-regulation of cyclin-dependent kinase 5 attenuates p53-dependent apoptosis of hippocampal CA1 pyramidal neurons following transient cerebral ischemia. *Sci. Rep.* **9**, 13032 (2019).

148. K. J. Smillie, M. A. Cousin, Dynamin I phosphorylation and the control of synaptic vesicle endocytosis. *Biochem. Soc. Symp.* **72**, 87–97 (2005).
149. T. Sun, X.-S. Wu, J. Xu, B. D. McNeil, Z. P. Pang, W. Yang, L. Bai, S. Qadri, J. D. Molkentin, D. T. Yue, L.-G. Wu, The role of calcium/calmodulin-activated calcineurin in rapid and slow endocytosis at central synapses. *J. Neurosci.* **30**, 11838–11847 (2010).
150. A. M. Walter, K. Wiederhold, D. Bruns, D. Fasshauer, J. B. Sørensen, Synaptobrevin N-terminally bound to syntaxin-SNAP-25 defines the primed vesicle state in regulated exocytosis. *J. Cell Biol.* **188**, 401–413 (2010).
151. H. Wang, D. R. Storm, Calmodulin-regulated adenylyl cyclases: Cross-talk and plasticity in the central nervous system. *Mol. Pharmacol.* **63**, 463–468 (2003).
152. Z. Wu, S. T. Wong, D. R. Storms, Modification of the calcium and calmodulin sensitivity of the type I adenylyl cyclase by mutagenesis of its calmodulin binding domain. *J. Biol. Chem.* **268**, 23766–23768 (1993).
153. R. Zdanowicz, A. Kreutzberger, B. Liang, V. Kiessling, L. K. Tamm, D. S. Cafiso, Complexin binding to membranes and acceptor t-SNAREs explains its clamping effect on fusion. *Biophys. J.* **113**, 1235–1250 (2017).
154. A. R. Quintana, D. Wang, J. E. Forbes, M. N. Waxham, Kinetics of calmodulin binding to calcineurin. *Biochem. Biophys. Res. Commun.* **334**, 674–680 (2005).
155. H. Schmidt, K. M. Stiefel, P. Racay, B. Schwaller, J. Eilers, Mutational analysis of dendritic  $\text{Ca}^{2+}$  kinetics in rodent Purkinje cells: Role of parvalbumin and calbindin D-28k. *J. Physiol.* **551**, 13–32 (2003).
156. S. V. Georgiev, S. O. Rizzoli, Phluorin-conjugated secondary nanobodies as a tool for measuring synaptic vesicle exocytosis and endocytosis. *Sci. Rep.* **15**, 10093 (2025).

**Acknowledgments:** We are extremely grateful to P. Puchenkov of the Scientific Data Visualization Support service, Research Support Division, Okinawa Institute of Science and Technology Graduate University for invaluable help in designing and coding the visualization of the model in Blender. **Funding:** This work was funded in part by a Grants-in-Aid for Scientific Research (KAKENHI) grant awarded to A.R.G., I.H., and E.D.S. (grant number: 20K06593) and in part by the Okinawa Institute of Science and Technology Graduate University. The work was also funded in part by grants from the German Research Foundation (Deutsche Forschungsgemeinschaft, DFG) SFB1286/A03/B02 to S.O.R. **Author contributions:** Writing—original draft: A.R.G. Conceptualization: A.R.G., S.O.R., and E.D.S. Investigation: A.R.G., S.V.G., and S.O.R. Writing—review and editing: A.R.G., S.O.R., and E.D.S. Methodology: A.R.G., I.H., and S.O.R. Resources: S.O.R. and E.D.S. Funding acquisition: A.R.G., I.H., S.O.R., and E.D.S. Data curation: I.H. Validation: A.R.G., I.H., and S.O.R. Supervision: S.O.R. and E.D.S. Formal analysis: A.R.G., S.V.G., and S.O.R. Software: I.H. and S.O.R. Project administration: S.O.R. and E.D.S. Visualization: A.R.G. and S.O.R. **Competing interests:** The authors declare that they have no competing interests.

**Data and materials availability:** All data needed to evaluate the conclusions in the paper are present in the paper and/or the Supplementary Materials. The data used to generate the figures in the paper can be accessed at <https://doi.org/10.5281/zenodo.13938271>. The model code, including the mesh, and instructions for running the model are available on ModelDB (model no. 2018007 available at <https://modeldb.science/2018007>).

Submitted 27 May 2024

Accepted 22 April 2025

Published 28 May 2025

10.1126/sciadv.adq6477